



HAL
open science

Nucleolar localization of the yeast RNA exosome subunit Rrp44 hints at early pre-rRNA processing as its main function

Ellen Okuda, Fernando Gonzales-Zubiato, Olivier Gadal, Carla Oliveira

► To cite this version:

Ellen Okuda, Fernando Gonzales-Zubiato, Olivier Gadal, Carla Oliveira. Nucleolar localization of the yeast RNA exosome subunit Rrp44 hints at early pre-rRNA processing as its main function. *Journal of Biological Chemistry*, 2020, 295 (32), pp.11195-11213. 10.1074/jbc.RA120.013589 . hal-04830100

HAL Id: hal-04830100

<https://cnrs.hal.science/hal-04830100v1>

Submitted on 10 Dec 2024

HAL is a multi-disciplinary open access archive for the deposit and dissemination of scientific research documents, whether they are published or not. The documents may come from teaching and research institutions in France or abroad, or from public or private research centers.

L'archive ouverte pluridisciplinaire **HAL**, est destinée au dépôt et à la diffusion de documents scientifiques de niveau recherche, publiés ou non, émanant des établissements d'enseignement et de recherche français ou étrangers, des laboratoires publics ou privés.



Distributed under a Creative Commons Attribution - NonCommercial 4.0 International License

Nucleolar localization of yeast RNA exosome subunit Rrp44 hints early pre-rRNA processing as its main function

Ellen K. Okuda¹, Fernando A. Gonzales-Zubiarte^{1#}, Olivier Gadal² and Carla C. Oliveira^{1*}

From the ¹Department of Biochemistry, Institute of Chemistry, University of São Paulo, SP, Brazil;

²Laboratoire de Biologie Moléculaire Eucaryote, Centre de Biologie Intégrative (CBI), Université de Toulouse, CNRS, UPS, 31000 Toulouse, France.

Running title: Exosome is concentrated in the yeast nucleolus

[#]Present address: School of Biological Sciences and Engineering, Yachay Tech University, Ecuador.

*To whom correspondence should be addressed: Carla C. Oliveira: Department of Biochemistry, Institute of Chemistry, University of São Paulo, São Paulo, SP 05508-000, Brazil; ccoliv@iq.usp.br; Tel. (55) 11 3091-9197. *Corresponding author

Keywords

Yeast RNA exosome; Rrp44; pre-rRNA processing; protein nuclear import; ribosome maturation.

ABSTRACT

The RNA exosome is a multi-subunit protein complex involved in RNA surveillance of all classes of RNA, and essential for pre-ribosomal RNA processing. The exosome is conserved throughout evolution, present in archaea and eukaryotes from yeast to humans, where it localizes to the nucleus and cytoplasm. Despite being considered as a protein present in these two subcellular compartments, here we show that the yeast exosome catalytically active subunit Rrp44/Dis3 not only localizes mainly to the nucleus, but is concentrated in the nucleolus, where the early pre-rRNA processing reactions take place. Moreover, we show by confocal analysis that core exosome subunits Rrp41 and Rrp43 also localize largely to the nucleus and are concentrated in the nucleolus. The results shown here shed more light on the localization of the yeast exosome and have implications regarding the main function of this RNase complex, which seems to be primarily related to early pre-rRNA processing and surveillance.

INTRODUCTION

The RNA exosome is a protein complex that participates in processing and degradation of all classes of RNA in eukaryotes (1,2). In *Saccharomyces cerevisiae*, the exosome is composed of a nine-subunit core (Exo9) that contains a heterohexameric ring formed by the subunits Rrp41, Rrp42, Rrp43, Rrp45, Rrp46 and Mtr3, and a heterotrimeric “cap” formed by the subunits Rrp4, Rrp40 and Csl4. Although

the structure of the exosome core is conserved from archaea to eukaryotes, it has no catalytic activity in the latter (3). In yeast, Exo9 interacts with Rrp44/Dis3 in the nucleus and cytoplasm to form a 10-subunit complex (Exo10). Rrp44 is an RNase II family member, and has two catalytic sites, one with endoribonucleolytic activity (PIN) and a second with processive 3'-to-5' exoribonucleolytic activity (RNB) (4-6). In yeast, the nuclear exosome contains Rrp6 (forming Exo11), an extra catalytic subunit with a distributive 3'-to-5' exoribonuclease activity that binds to the trimeric cap and upper portion of the hexameric ring, opposite to the Rrp44 binding site. Rrp6 is the only nonessential exosome subunit, although the deletion of its gene results in a slow growth phenotype, temperature sensitivity, filamentous growth and RNA processing defects (7-12).

Ribosome biogenesis involves the coordinated transcription, surveillance, modification, and processing of precursor rRNAs, which undergo modifications and several exo- and endonucleolytic cleavage reactions during its maturation process (13,14). In the canonical pre-rRNA maturation pathway, the RNA exosome complex is responsible for the degradation of the spacer sequence 5'-ETS after cleavage at A₀, and for the 3'-5' end processing of 7S pre-rRNA to the mature 5.8S rRNA (Fig. S1A) (8,15). The 5'-ETS is released co-transcriptionally and completely degraded by the exosome, while SSU processome is formed by association of U3 snoRNP and other

factors to the pre-rRNA being transcribed (16). Later during pre-rRNA processing, endonucleolytic cleavage at C₂ site in ITS2 of pre-rRNA 27S separates pre-rRNAs 7S (5.8S + 5' region of ITS2) and 26S (3' region of ITS2 plus 25S) (17), which undergo exonucleolytic processing by the exosome and Rat1/Rai1, respectively, to generate mature rRNAs 5.8S and 25S (17,18). Mtr4 and the RNA exosome are essential for the ITS2 processing of 7S after the cleavage at C₂ (18), when the exosome subunit Rrp44 shortens 7S to the intermediate 5.8S+30, which is then handed over to Rrp6 that trims it to 6S pre-rRNA, which gives rise to the mature 5.8S rRNA after further processing in the cytoplasm (19). Exosome is also involved in quality control steps of rRNA processing, targeting 23S rRNA generated by direct cleavage at A₃ site for degradation, and unprocessed 35S rRNA (Fig. S1B) (20-22).

Although the structure and function of the exosome has been extensively studied in recent years, detailed information on the mechanisms responsible for the subcellular localization of its different forms is still lacking. Despite the identification of some of the exosome subunits in the nucleolus (23), the core subunits of this complex are regarded as mainly present in nucleus and cytoplasm (3,9,23,24). Rrp4 and Rrp6 have been reported to be present in nucleus and nucleolus, in addition to the cytoplasm in the case of Rrp4 (9). We have recently identified the nuclear import mechanisms for Rrp6 and shown that this exclusively nuclear subunit has multiple transport pathways, being bound by the α -importin Srp1 and β -importins Kap95 and Sxm1 (12). To gather more information on the transport of the exosome to the nucleus, we investigated the nuclear import pathway of the other exosome catalytically active subunit, Rrp44, and show here that importins Srp1 (α) and Kap95 (β), respectively, are responsible for this transport, which occurs independently of Rrp6. Furthermore, we show that the exosome complex is highly concentrated in the nucleus, and more specifically in the nucleolus, where pre-rRNA is transcribed and where the early processing reactions take place.

Results

One of the essential functions of the exosome in yeast is the processing of pre-rRNA in the nucleus, which underlines the relevance of uncovering the mechanism of nuclear import

that allows this protein complex to enter the nucleus. We have previously shown that one of the exosome active subunits, Rrp6, is transported to the nucleus by the karyopherins Srp1/Kap95 or Sxm1 (12), but information on the other catalytically active exosome subunit, Rrp44/Dis3, nuclear transport is lacking. Rrp44 has five distinct structural domains: an endonuclease PinC N-terminal domain, two CSD cold shock domains, an essential exoribonuclease domain, RNB, and an RNA binding domain S1 (6). Based on software analyses (see Experimental procedures section), we identified the presence of three putative Nuclear Localization Signals (NLSs) in the amino acidic sequence of Rrp44 (named here NLS1, NLS2 and NLS3), each overlapping one of the functional domains PinC, CSD2, and S1, respectively (Fig. 1).

NLS1 is a nuclear localization signal known as the PY-NLS, located in the PinC domain of Rrp44 between the residues 172 and 188 (¹⁷²RAIRKTCQWYSEHLKPY₁₈₈). A weak consensus motif composed of an N-terminal hydrophobic or basic motif and a C-terminal R/H/KX₂₋₅PY recognized by importins Kap104, Sxm1/Kap108, Kap121, Kap114, Nmd5/Kap119, and Kap95 (25-27). NLS2 is located in CSD2 domain between the residues 370 and 401 (³⁷⁰RRL₁LAKDAMIAQRSKKIQPTAKV₁VYI₁QRRSW₁R₄₀₁) and contains the consensus NLS R/KX₂LX_nV/YX₂V/IXK/RX₃K/R recognized by the importins Kap114, Kap95, Kap123, Pse1, and Kap104 (28). NLS3 is located at the C-terminus of Rrp44 between the residues 988 and 1001 (⁹⁸⁸DPITSKRKAELLLK₁₀₀₁). The prediction of this NLS is based on its similarity to the *Drosophila* Rrp44 (dDis3), which is recognized by importin alpha3 (29,30). These findings suggest that Rrp44 could be transported to the nucleus independently of other exosome subunits.

NLS1 is essential for nuclear import

To explore the importance of each of Rrp44 NLSs for its nuclear import, we constructed plasmids for episomal expression of mutant versions of Rrp44 (Fig. 1). Rrp44 variants were fused to GFP at the N-terminus and expressed under control of *MET25* promoter, strongly induced in absence of methionine. Analysis of the subcellular localization by fluorescence microscopy shows that despite being considered a nuclear and

cytoplasmic protein (5,35), full-length GFP-Rrp44 was found mainly concentrated in the nucleus (Fig. 2A), in agreement with high-throughput analyses (23).

Analysis of the subcellular localization of Rrp44 deletion and point mutants showed a variety of phenotypes depending on the presence of any of the putative NLS described above. Rrp44 mutants containing NLS1 in their sequence localized exclusively to the nucleus (Rrp44₁₋₉₈₅, Rrp44₁₋₄₇₅, Rrp44_{R397A,R398T}, Rrp44_{P187A,Y188A}) or concentrated in the nucleus, but were also present in the cytoplasm (Rrp44_{Δ364-407}, Rrp44₍₁₋₃₆₃₎₍₄₀₈₋₉₈₅₎, Rrp44₁₋₂₁₈) (Fig. 2). Mutant Rrp44₁₋₂₁₈ displayed two distinct phenotypes, some of the cells showed the protein concentrated in the nucleus, while others showed small cytoplasmic foci, which could correspond to degradation sites (Fig. 2B; Fig. S2). Despite the point mutations in PY-NLS, mutant Rrp44_{P187A,Y188A} still concentrates in the nucleus, indicating that the remaining sequence suffices for importin recognition. Mutants lacking NLS1, although present in the nucleus, showed strong signal in cytoplasm (Rrp44₂₃₆₋₄₇₅, Rrp44₄₇₅₋₁₀₀₁). Mutant Rrp44₂₃₆₋₄₇₅ that contains only NLS2, showed the same phenotype as GFP alone, whereas Rrp44₄₇₅₋₁₀₀₁ was present in cytoplasm, but concentrated in the nucleus in some cells (Fig. 2B).

Mutants lacking NLS2, Rrp44_{Δ364-407} and Rrp44₍₁₋₃₆₃₎₍₄₀₈₋₉₈₅₎ localized to the nucleus, which could suggest that NLS2 is not important for Rrp44 nuclear import. However, despite being concentrated in the nucleus, these mutants showed detectable signals in the cytoplasm (Fig. 2A), leading to the suggestion that in the absence of NLS2, Rrp44 is still transported to the nucleus but not very efficiently. Absence of the C-terminal NLS3, on the other hand, does not affect Rrp44 nuclear localization, since both mutants Rrp44₁₋₉₈₅, and Rrp44₁₋₄₇₅, which lack NLS3, localized exclusively to the nucleus, and Rrp44₍₁₋₃₆₃₎₍₄₀₈₋₉₈₅₎, which lacks NLS2 and NLS3, was concentrated in the nucleus (Fig. 2A).

Based on these results showing that deletion mutants containing NLS1 localize to the nucleus, whereas mutants lacking NLS1 are present in nucleus and cytoplasm (Fig. 2; Fig. S3), we can conclude that presence of NLS1 plus either NLS2 or NLS3 is sufficient for Rrp44 nuclear localization. Hence, NLS1 would be the most important signal for Rrp44 nuclear import.

The expression of these deletion and point mutants of Rrp44 was analyzed by western blot of total cell extracts, which shows that most of the mutants are expressed at similar levels in yeast, and the protein bands detected have the expected molecular masses (Fig. 3). The ability of these mutants to complement growth of *Δrrp44/GAL::RRP44* cells was tested by expressing the GFP-fused Rrp44 mutants in this conditional strain, growing on galactose or glucose media (expression or depletion of Rrp44, respectively). Toxicity of GFP-Rrp44 variants was evaluated with the expression of wild-type Rrp44 (galactose) in the presence or absence of methionine for lowering or increasing the expression of the variants, respectively. The results show that point mutants Rrp44_{R397A,R398T} (NLS2 mutant) and Rrp44_{P187A,Y188A} (NLS1 mutant), which localize to the nucleus, fully complement growth of *Δrrp44/GAL::RRP44* on glucose, similar to GFP-Rrp44 (Fig. 4). Deletion mutant Rrp44₁₋₉₈₅, which lacks NLS3, but localizes to the nucleus, also complements growth. These results reinforce those presented above, that the Rrp44 mutants transported to the nucleus are functional. Confirming the results of protein localization, mutants Rrp44_{Δ364-407} and Rrp44₍₁₋₃₆₃₎₍₄₀₈₋₉₈₅₎ partially complement growth of *Δrrp44/GAL::RRP44* on glucose. Despite being transported to the nucleus, mutants with further deletions in Rrp44 sequence, resulted in nonfunctional proteins (Fig. 4). Interestingly, co-expression of GFP-Rrp44 at high levels (Gal) and functional Rrp44 mutants (-Met) led to slow growth, contrary to what was seen on glucose (Fig. 4). Addition of methionine to the medium alleviates this effect, increasing growth. These results suggest that high levels of Rrp44, combined with high levels of GFP-Rrp44, are deleterious to the cells. Mutant Rrp44₃₆₄₋₁₀₀₁, which showed dominant negative effects, strongly inhibiting growth in all conditions, and displayed various localization phenotypes (Fig. 4 and data not shown), and mutant Rrp44_{Δ526-987}, which was not detected by western blot, were therefore not further analyzed.

These growth complementation results are consistent with the analysis of pre-ribosomal RNA processing on glucose, when GFP tagged Rrp44 variants are expressed in absence of wild-type Rrp44. As a control, rRNA processing was analyzed in the presence of WT Rrp44 (Galactose). In the absence of Rrp44, 7S

rRNA accumulates, without accumulation of detectable 5.8S+30 species. In the absence of Rrp6, 7S processing by Rrp44 leads to strong accumulation of 5.8S+30 rRNA (detected with both probes P1 and P2). Point mutants Rrp44^{P187A,Y188A} and Rrp44^{R397A,R398T} fully complement the depletion of wild type Rrp44, visualized by the efficient processing of 7S pre-rRNA and formation of mature 5.8S rRNA (Fig. 5). Expression of the mutants Rrp44¹⁻²¹⁸ (PIN domain), Rrp44²³⁶⁻⁴⁷⁵ (CSD1 + CSD2), or Rrp44¹⁻⁴⁷⁵ (PIN + CSD1 + CSD2) leads to processing defects, with accumulation of pre-rRNA 7S and consequent decreased levels of mature 5.8S rRNA. Interestingly, mutant Rrp44¹⁻⁴⁷⁵ accumulates at low level an intermediate very similar to 5.8S+30, which is a characteristic of strains lacking Rrp6 (Fig. 5). Note that such rRNA species are better detected with P2, which hybridizes to ITS2 region. In addition to 5.8S+30, mutants Rrp44^{Δ364-407} and Rrp44⁽¹⁻³⁶³⁾⁽⁴⁰⁸⁻⁹⁸⁵⁾ also accumulate intermediates longer than 5.8S+30 (Fig. 5). Mutant Rrp44⁴⁷⁵⁻¹⁰⁰¹ (RNB + S1 domains), on the other hand, shows lower levels of pre-rRNA 7S and of mature 5.8S (Fig. 5). These results suggest that Rrp44⁴⁷⁵⁻¹⁰⁰¹ may not associate stably with the exosome core, decreasing the efficiency of 7S processing, but may be free to degrade RNAs, leading to the decreased levels of both precursor and mature rRNAs. An overview of the phenotypes of the Rrp44 mutants relative to wildtype is shown in Fig. S5.

Rrp44 is transported to the nucleus by karyopherins Kap95 and Srp1

In order to better understand the nuclear import pathway of Rrp44 and to identify the karyopherins involved in this process, GFP-Rrp44 was expressed in strains with mutated karyopherin genes, chosen based on the putative NLSs present in Rrp44 sequence. Deletion mutants of the non-essential karyopherins Sxm1, Kap123, and Kap114 were transformed with a plasmid coding for GFP-Rrp44 and the subcellular localization of this protein was analyzed by fluorescence and confocal microscopy. The results show that none of these karyopherins affects Rrp44 localization (Fig. S6 and data not shown). Lowering levels of Srp1 or Kap95 by incubating the strains *Δsrp1/GAL::SRP1* and *Δkap95/GAL::KAP95* on glucose medium, on the other hand, strongly affects GFP-Rrp44 localization, leading to partial mislocalization of this protein to the

cytoplasm, despite still being concentrated in the nucleus (Fig. 6). These results indicate that Kap95 and Srp1 are the main karyopherins involved in nuclear import of Rrp44.

Since Srp1 and Kap95 affected Rrp44 localization, physical interaction between these proteins was analyzed by co-immunoprecipitation after expression of GFP-Rrp44 and protein A-tagged karyopherins in yeast. The results show that both A-Srp1 and A-Kap95 co-immunoprecipitate GFP-Rrp44 (Fig. 7A), confirming the interaction between these proteins and the involvement of Srp1 and Kap95 in the nuclear transport of Rrp44. Since the GFP tag alone was also detectable in the elution fractions, to exclude that interaction was due to GFP, an additional experiment was performed, in which extracts from yeast cells expressing GFP or GFP-Rrp44 were incubated with IgG-sepharose without previous incubation with the karyopherins. After extensive washing, eluted proteins were analyzed by western blot, which shows that GFP binds unspecifically the resin with much higher affinity than GFP-Rrp44 (Fig. S4B), accounting for the background binding detected in the co-immunoprecipitation experiments (Fig. 7A). These results are in agreement with global protein interaction data that indicated protein complexes containing both Rrp44 and Srp1 (31,32).

To determine whether Srp1 and Kap95 were capable of interacting directly with Rrp44 *in vitro*, protein pull-down assays were performed. Recombinant GST-Rrp44 was immobilized on glutathione-sepharose beads and then incubated with His-Kap95 or His-Srp1. Fractions were separated by SDS-PAGE and subjected to western blot with antibodies against the His and GST tags. The results show the direct interaction between GST-Rrp44 and His-Kap95 (Fig. 7B). Although His-Kap95 is also pulled-down with GST, it binds more efficiently GST-Rrp44, as indicated by the intensity of the bands detected in elution fractions. His-Srp1, however, was not detected in the elution (Fig. 7B, lower panel). These results suggest that Kap95 binds Rrp44 NLS, being responsible for its nuclear transport. Srp1 may indirectly interact with Rrp44, depending on β -importins such as Kap95 to recognize this cargo protein. Combined, the results shown here strongly indicate that Rrp44 is transported to the nucleus by a Kap95 dependent import

pathway, either by itself, complexed with Srp1, or with another β -karyopherin.

Nuclear transport of the exosome complex

Although Rrp6 has been shown to have multiple NLS and transport pathways (12), it is generally not considered to be responsible for the nuclear import of other exosome subunits because it is not an essential yeast protein. The lack of effect of Rrp6 on nuclear transport of core exosome subunits was confirmed here upon analysis of subcellular localization of Rrp44, Rrp41 and Rrp43 in $\Delta rrp6$ cells (Fig. S7). Upon identifying NLS in Rrp44, we analyzed whether this essential exosome subunit influences the nuclear import of other exosome subunits. The episomal GFP-fused exosome subunits Rrp6, Rrp41, and Rrp43 were expressed in $\Delta rrp44/GAL::RRP44$ either in the presence (Gal) or upon depletion of Rrp44 (Glu). Contrary to Rrp6 and Rrp44, Rrp41 and Rrp43 expressed under the strong *MET25* promoter are present in both nucleus and cytoplasm. Depletion of Rrp44 does not significantly affect the localization of these exosome subunits (Fig. 8), suggesting independent nuclear transport pathways. The non-affected GFP-Rrp6 localization in the absence of Rrp44 was expected given the already described nuclear import pathways of Rrp6 (12). Control experiments in WT cells confirm that when overexpressed using episomal genes under control of *MET25* promoter, Rrp41 and Rrp43 localize to the nucleus and cytoplasm (Fig. S8). Overexpressed Rrp44 and Rrp6, on the other hand, show nuclear localization (Fig. S8).

Exosome subcellular localization

Curiously, as shown here, Rrp44 is mainly nuclear, whereas the exosome RNase PH ring subunits Rrp41 and Rrp43 show a nuclear and cytoplasmic localization. To determine whether this phenotype is due to the overexpression of the exosome subunits coded in multicopy plasmid under control of the strong *MET25* promoter, chromosomal C-terminally tagged GFP-fused exosome subunits genes, under control of their endogenous promoters, were constructed for Rrp44, Rrp6, Rrp41 and Rrp43. No growth defect was observed, showing that C-terminally tagged proteins expressed at endogenous levels remain functional. Although the subunits of Exo10 are considered to be present both in nucleus and

cytoplasm (9), the results shown here demonstrate that the core subunits Rrp41 and Rrp43, and the catalytically active subunits Rrp44 and Rrp6 are all concentrated in the nucleus (Fig. 9). These proteins expressed at endogenous levels are visible almost exclusively in the nucleus, and more strikingly, are concentrated in the nucleolus (Fig. 9). Importantly, analyses using confocal microscopy and quantification of sum of fluorescent signal, followed by projection along Z-axis of all acquired confocal images and calculation of enrichment of the exosome signal in each cellular compartment (see Experimental procedures), corroborates the nucleolar localization of the exosome. Exosome concentration in the nucleoplasm is 6 to 9 times higher than in the cytoplasm, while nucleolar exosome concentration is 10 to 20 times higher than in the cytoplasm (Fig. 9).

Careful inspection of individual Z section of the acquired fluorescent images, however, shows that despite being concentrated in the nucleolus, the exosome subunits localization is slightly different from that of RNA polymerase I (Rpa190), as if in a different sub-nucleolar compartment (Fig. 10). These results strongly suggest that in the nucleolus, nascent rRNAs are exposed to high concentration of exosome in a “processing compartment” adjacent, but distinct from RNA polymerase I, for processing and quality control of pre-rRNAs.

Discussion

The RNA exosome was first identified in *Saccharomyces cerevisiae* as an RNase involved in maturation and quality control of stable RNAs (8,15). In the subsequent studies, it became clear that the exosome is a protein complex conserved throughout evolution, which is present in the nucleus and cytoplasm of eukaryotic cells, where it interacts with many cofactors and participates in different RNA processing and degradation pathways (3,33,34).

In yeast, Exo10, composed of the exosome core and Rrp44, is considered to be present both in nucleus and cytoplasm, participating in different reactions in each of these subcellular compartments (35). We have previously identified the nuclear import pathways of Rrp6 and shown that this nuclear exosome subunit has redundant mechanisms of transport to the nucleus, directly interacting

with α -importin Srp1 and β -importins Kap95 and Sxm1 (12). To better understand the mechanism of exosome assembly and transport to the nucleus, where this complex participates in the essential process of ribosome maturation, we investigated here the nuclear import pathway of the other catalytically active exosome subunit, Rrp44.

We identified three putative nuclear localization signals (NLSs) in the primary sequence of Rrp44 and constructed deletion and point mutants to determine the Rrp44 sequences mediating its transport to the nucleus. We show evidence that NLS1 is the most important sequence, but not the only NLS, for the nuclear import of Rrp44, which suggests that different karyopherins may bind Rrp44 for directing it to the nucleus. Depletion of Kap95 strongly affects the nuclear localization of Rrp44, and accordingly, NLS1 contains the consensus sequence for Kap95 binding, a PY-NLS (36). However, point mutant Rrp44^{P187A,Y188A} still localizes to the nucleus, suggesting that additional signals are recognized by Kap95. Although Srp1 also affects Rrp44 transport to the nucleus, a classical NLS was not found in Rrp44 sequence, suggesting that Srp1 could recognize a non-consensus NLS, or that the transport is mediated by Kap95/Srp1 heterodimer upon recognition of the NLS by Kap95, or by an additional β -karyopherin.

Rrp44 has endo- and exonucleolytic activities (5,37), and is involved pre-rRNA processing in nucleus and nucleolus (8). The mutants that contain the exonuclease domain of Rrp44 and at least two of the putative NLSs, localize to the nucleus and complement growth of the $\Delta rrp44/GAL::A-RRP44$ strain. Analysis of pre-rRNA processing in the mutants show that the mutants that do not localize to the nucleus, or that do not contain the RNB domain, display a defective pre-rRNA processing phenotype, with accumulation of intermediates with sizes in the range between pre-rRNAs 7S and 5.8S+30. Importantly, these intermediates are not substrate for Rrp6, which processes the product of Rrp44 reaction, 5.8S+30 (7). The intermediates accumulating in the presence of non-functional Rrp44 mutants, have longer extensions at the 3'-end than 5.8S+30, and have also been observed in mutants of core exosome subunits (8). Interestingly, Mutant Rrp44⁴⁷⁵⁻¹⁰⁰¹ (containing RNB + S1 domains, but lacking PIN and CSD domains) shows decreased levels of both precursor and mature rRNAs. These

results are in agreement with Rrp44 structural data showing that PIN and CSD domains are responsible for the stable interaction between Rrp44 and the RNase PH ring of the exosome (38). Rrp44 lacking these domains may not associate stably with the exosome, decreasing the efficient processing of 7S, but instead, may be free and more active to degrade RNAs (39,40).

As shown here, depletion of Rrp44 does not affect nuclear localization of Rrp6, as expected, given that Rrp6 has its own NLSs (12), and does not directly interact with Rrp44 (38,40). Interestingly, depletion of Rrp44 does not affect localization of episomal core exosome subunits either, suggesting a different mechanism of transport for the remaining subunits of this complex.

The most striking results coming from the analyses described here are the very low concentration in the cytoplasm of all the exosome subunits analyzed. Exosome is not only concentrated in the nucleus, but specifically in the nucleolus. This information is relevant in light of the function of the yeast exosome. In the cytoplasm, the exosome participates in the minor pathway of mRNA decay, degrading 3'-5' deadenylated mRNAs (41-43). The major pathway of cytoplasmic mRNA degradation in yeast does not involve the exosome, and starts with deadenylation of mRNAs by the Ccr4-Not complex (41,44,45), followed by decapping by Dcp1 (46,47) and 5'-3' degradation by Xrn1 (48,49). Pre-rRNA processing and surveillance, on the other hand, starts in the nucleolus and continues to the nucleoplasm, as the pre-ribosomal particles are concomitantly transported towards the cytoplasm (50). Interestingly, in spite of the intricate protein interactions involved in 7S pre-rRNA processing, 60S subunits bearing 7S have been identified in polysomes (51).

As soon as 5'-ETS is released after co-transcriptional cleavage of pre-rRNA at sites A₀-A₁, the exosome can degrade it in the nucleolus, after being recruited there by SSU processome factors (50,52-54). The results shown here reinforces the importance of the exosome for pre-rRNA processing and quality control, by showing that the exosome is mainly concentrated in the nucleolus. The concentration of the exosome in the nucleolus also corroborate recent data showing the interaction of exosome subunits with pre-ribosomal particles 90S, pre-40S and pre-60S,

interactions which were stabilized by the inhibition of pre-rRNA processing by the depletion of pre-60S factor Nop53 (55).

As we also show here, the nucleolar concentration of the exosome subunits can only be appreciated when the GFP-fused proteins are expressed at endogenous levels. Overexpression of these proteins in plasmid-based systems lead to the visualization of weak signals in the cytoplasm and very strong nuclear signals, overshadowing the nucleolus.

Not only were the exosome subunits concentrated in the nucleolus, but careful high-resolution analysis of protein localization showed that when comparing to RNA polymerase I subunit Rpa190 on individual Z-section of spinning disk confocal microscopy, the exosome subunits do not exactly overlap Rpa190, suggesting a slightly different localization. Interestingly, recent data on mammalian cells show that the box C/D snoRNP subunit Fibrillarin that is also part of SSU processome, does not exactly colocalizes with RPA194, but rather show a phase separation between rRNA transcription and processing (56). Our results could suggest that transcribed rRNA is co-transcriptionally processed in an associated compartment containing the exosome.

In summary, here we show that the exosome catalytic subunit Rrp44 is transported to the nucleus independently of other subunits. Importantly, we show that the yeast exosome is concentrated in the nucleolus, in a sub-compartment flanking but different from RNA polymerase I, placing the exosome in the early phases of pre-rRNA processing.

Experimental procedures

Construction of strains and yeast growth condition

Yeast maintenance and growth was performed in YPD medium (1% yeast extract, 2% peptone and 2% glucose), or YNB medium (0.67% yeast nitrogen base, 0.5% (NH₄)₂SO₄ and 2% glucose or galactose) supplemented with the required amino acids. Plasmids constructed in this study, described in Table 1, were built according to standard cloning techniques and sequenced by the Big Dye method (PerkinElmer Life Sciences). Plasmids expressing the GFP fusions in yeast were constructed by inserting DNA fragments into pUG34 plasmid (57) using oligonucleotides

with specific restriction sites (sequences available upon request). Expression of these GFP fusions was regulated by *MET25* promoter. Rrp44 point mutations were obtained by site-directed mutagenesis (Stratagene or In-Fusion - Takara) using plasmid pUG34-RRP44 as template and oligonucleotides containing the respective mutations. Plasmid pRS305-NUP57-tDimerRFP (58) was constructed as follows. NUP57 was amplified as two overlapping PCR fragments (primer pairs 1568/1570 and 1569/1571-matrix strain BY4741). The two PCR fragments were mixed and used as matrix with primers 1568/1571 to amplify full length NUP57 with an internal BglIII site. NUP57 containing fragment was cloned in pRS305-NUP2-tDimerRFP (59) as a NotI-BamHI fragment. To construct Nup57 t-dimer genomic tagged strain, the plasmid pRS305-Nup57-tDimer was linearized with BglIII and inserted by homologous recombination in a BY4742 strain. It was selected for leucine prototrophy, and checked by fluorescence microscopy. Plasmid pFA6-mCherry-KIURA3 was constructed by cloning into pFA6-GST-KIURA3 PacI-AscI mCherry a fragment from pFA6-mCherry-HIS3.

Haploid strain $\Delta rrp44/YCplac33-GAL::A-RRP44$ was obtained after sporulation of the diploid strain $RRP44/\Delta rrp44$ previously transformed with plasmid $YCplac33-GAL::A-RRP44$.

Strains bearing genomic insertion of GFP or mCherry were constructed by amplifying a PCR cassette containing *URA3* gene from *K. lactis* as selectable marker and GFP-tag or mCherry-tag sequence from the plasmid pFA6-GFP(S65T)-KIURA3 or pFA6-mCherry-KIURA3, respectively. The PCR fragment was inserted by homologous recombination downstream each protein gene bearing a TAP-tag (60) using the Swap-tag method (61). Transformants were selected for uracil prototrophy and checked by PCR of the targeted genomic loci, and analyzed by fluorescence microscopy. BY4742 strains bearing Rrp44 fused to GFP or mCherry were constructed as described (62). Similarly, Rpa190 fused to mCherry was constructed as described (62).

RPA190 was also genomic tagged with mCherry in exosome GFP-tagged strains and BY4742 strain. The same strategy was used by first amplifying the plasmid pFA6-mCherry-HIS3, then inserting it in the genome by

homologous recombination and selecting for histidine prototrophy.

Nuclear localization signal identification

The software packages PSORT II Prediction (<http://www.genscript.com/psort/psort2.html>), cNLS Mapper (Kosugi et al., 2009) and NLStradamus (63) were used to predict the presence of Nuclear Localization Signals (NLSs) in the amino acidic sequence of Rrp44.

Fluorescence microscopy on fixed cells

For protein depletion based on *GALI* promoter, cells were inoculated either in selective galactose or glucose medium and incubated for 14 to 16 hours to exponential phase. For microscopy analysis, cells were fixed in 70% methanol for 15 min, rinsed with cold PBS, and then treated with 1 mg/ml RNase for 30 min. Cells were observed using a Nikon Eclipse Ti microscope equipped with filters for green fluorescence (GFP-3035B-000-ZERO, Semrock) and red fluorescence (Texas Red BrightLine set, TXRED4040-B, Semrock). The exposure times varied from 1 to 3 s. Images were processed and analyzed using the programs Nis Elements (version 3.07; Nikon) and ImageJ (National Institutes of Health, Bethesda, MD). Confocal images were captured in a 1024 × 1024-pixel format using a Zeiss LSM 780 confocal laser-scanning inverted microscope (Carl Zeiss, Germany) at Research Facility Center (CEFAP-USP). Image stacks comprised eight images captured with an alpha Plan-Apochromat 100×/1.46 oil differential interference contrast M27 objective (Carl Zeiss), applying a zoom factor of 1.5. Step intervals along the *z* axis ranged from 200 to 250 nm. Image processing was performed using Zen 2011 software (version 11.00.190; Carl Zeiss).

Fluorescence microscopy on living cells

Exponentially growing yeast were collected, resuspended in synthetic complete medium (DIFCO), and observed in the fluorescence microscope. Confocal microscopy was performed using a Nipkow-disk confocal system (Revolution; Andor) installed on an Olympus microscope (IX-81), featuring a confocal spinning disk unit (CSU22; Yokogawa) and a cooled electron multiplying charge-coupled device camera (DU 888; Andor). The system was controlled using IQ 2 software (Andor). Images were acquired using

a 100× Plan Apo 1.4 NA oil immersion objective and a twofold lens in the optical path. Single laser lines used for excitation were diode-pumped solid-state lasers exciting GFP fluorescence at 488 nm (50 mW; Coherent) and mCherry fluorescence at 561 nm (50 mW; Cobolt jive), and a Dichroic mirror Di01-T405/488/568/647-13x15x0,5 was used; Semrock was used and a bi-bandpass emission filter (FF01-512/630-25; Semrock) allowed collection of the green and red fluorescence. In our conditions, pixel size was 65 nm. For quantification of nucleolar volume, *z* stacks of 40 images with a 200-nm *z* step were used. Exposure times varied from 0.1 to 1 s. Digital pictures were processed using ImageJ (National Institutes of Health, Bethesda, MD - <https://imagej.nih.gov/ij/>).

Image analysis and quantification

Confocal images were imported into ImageJ, signal intensities of GFP tagged proteins were measured and their subnuclear localizations were analyzed using a dedicated image analysis pipeline (ImageJ Macro). Cell area was determined based on transmission light thanks to the following step: background removal (subtracting Gaussian Blur image – sigma=40); segmentation of the cells with Moments threshold algorithm; determination of the objects corresponding to the cells with Analyze Particle (ImageJ function); separation of the cells in contact with Adjustable Watershed Plugin (https://imagejdocu.tudor.lu/doku.php?id=plugin:segmentation:adjustable_watershed:start). Nucleolar and nuclear segmentation was achieved using RNA polymerase I largest subunit Rpa190 tagged with mCherry, strongly enriched in the nucleolus, and detectable in the nucleoplasm. First, we applied a Sum Z-Projection to the initial mCherry Image. Then, to determine the nucleolus area in each cell, we used a Wavelet filter and finally segmented with Yen threshold algorithm. To determine the nucleus area, we directly segmented on the *Z* projected image a Triangle threshold algorithm. Cells were then divided in nucleolus, nucleoplasm and cytoplasm. ImageJ macro was used to quantify GFP signal in each compartment. All quantifications were performed relative to background fluorescence, measured using control cells with Rpa190 tagged with mCherry, but with no GFP expression.

To quantify exosome signal enrichment in each compartment, the mean signal of the entire cell was calculated: ((intensity of grey level in the cell – Background) /cell surface area). The mean cellular signal was used as a proxy to a homogeneous concentration in the entire cell. Each compartment mean signal measure was then divided by the mean cellular signal in each cell. The concentration ratio shows the enrichment of exosome signal per compartment, all relative to the mean signal of the entire cell.

Protein pulldown

Cellular extracts (generated in 20 mM Tris, 150 mM NaCl, 1 mM EDTA, 0.8% Nonidet, 1 mM DTT) of *E. coli* cells expressing either GST or GST-Rrp44 were incubated for 2h at 4°C with 60 µl of glutathione-Sepharose beads (GE Healthcare), and the unbound material was collected and beads washed with the same buffer. Beads were then incubated with cellular extracts containing His-Srp1 or His-Kap95, flow-through was collected, and beads were washed with the same buffer. Bound proteins were eluted with 50 mM Tris, pH 8.0, 10 mM reduced glutathione.

Co-Immunoprecipitation

Interaction of karyopherins Srp1 and kap95 with Rrp44 was tested by co-immunoprecipitation by using strains $\Delta kap95/GAL::A-KAP95$ and $\Delta srp1/GAL::A-SRPI$ transformed with pUG34 or pUG34-Rrp44. For each strain, 2L of cells were grown to an OD₆₀₀ ~1.0, and collected in Co-IP buffer (0,1% NP40, 150mM NaCl, 5mM EDTA, 50mM Tris-HCl pH7.5, 0.5x Halt Protease Inhibitor Cocktail (Thermo Scientific) (modified from (64))). Total yeast extracts were obtained with a Ball Mill device (Retsch, Mixer Mill MM 200 or Mixer Mill PM 100), and cleared by centrifugation at 40000 rpm for 1h at

4°C. Supernatant was then incubated for two hours at 4°C with IgG Sepharose 6 Fast Flow (GE Healthcare) previously equilibrated with Co-IP buffer. The resin was washed four times with 500µl of Co-IP buffer (twice with 150mM NaCl and twice with 250mM NaCl), followed by further wash with 100mM ammonia acetate, 0,1M magnesium chloride. Elution of the specific karyopherin was performed by incubation with 500 mM ammonium hydroxide for 20 min (65).

Immunoblotting experiments

Protein samples were resolved by SDS-PAGE and transferred to polyvinylidene difluoride (PVDF) or nitrocellulose (NC) membranes (GE Healthcare). Membranes were incubated with primary antibodies against GST (Sigma-Aldrich), His-tag (Sigma-Aldrich), GFP (Sigma-Aldrich), or Pgk1 (Abcam) in phosphate-buffered saline (PBS)/Tween 20/nonfat milk. Secondary antibodies used were anti-rabbit (IRDye 680RD) or anti-mouse IgG (IRDye 800CW) conjugated to fluorophore (Licor). Western blots were developed using Odyssey® Imaging Systems.

Northern hybridization

Total RNA was isolated from yeast cells by a modified hot phenol method (66). The RNA extract was quantified and 6 µg of denatured total RNA was loaded on gel. RNAs were separated by electrophoresis on 7% denaturing polyacrylamide gel, and transferred to Hybond nylon membrane (GE healthcare). Hybridization was performed using biotin-labeled or fluorescent probes specific to rRNAs. 5S rRNA and scR1 were used as controls. Quantification of bands from northern hybridizations were performed with Image J software.

Funding

This work was supported by a grant from Fundação de Amparo à Pesquisa do Estado de São Paulo (FAPESP - 15/06477-9 to C.C.O.), and by CBI (Centre de Biologie Integrative – Toulouse) to O.G. E.K.O. was supported by CNPq and by FAPESP fellowships (master's 17/17777-9) and Research Internships Abroad (18/19451-6) and CNRS (Centre National de la Recherche Scientifique). F.A.G. was supported by a FAPESP postdoctoral fellowship (12/50196-6).

Acknowledgements

We are grateful to all members of the Oliveira laboratory for help, reagents and discussion, especially L.P.P. Cepeda. We thank Frederico Gueiros Filho and members of his laboratory for the use of the fluorescence microscope. We also thank Mario Costa Cruz from CEFAP-USP for help with confocal microscopy and discussion. We are very grateful to Sylvain Cantaloube from the LITC imaging platform of Toulouse TRI and Image processing platform for his assistance and development of the image analysis pipeline. We acknowledge members of the Gadal's lab for help, advice and discussion, especially Isabelle leger-Silvestre, Christophe Dez and Lise Dauban.

References

1. Chlebowski, A., Lubas, M., Jensen, T. H., and Dziembowski, A. (2013) RNA decay machines: the exosome. *Biochim Biophys Acta* **1829**, 552-560
2. Schneider, C., and Tollervey, D. (2013) Threading the barrel of the RNA exosome. *Trends Biochem Sci* **38**, 485-493
3. Januszyk, K., and Lima, C. D. (2014) The eukaryotic RNA exosome. *Curr Opin Struct Biol* **24**, 132-140
4. Liu, Q., Greimann, J. C., and Lima, C. D. (2006) Reconstitution, activities, and structure of the eukaryotic RNA exosome. *Cell* **127**, 1223-1237
5. Dziembowski, A., Lorentzen, E., Conti, E., and Seraphin, B. (2007) A single subunit, Dis3, is essentially responsible for yeast exosome core activity. *Nat Struct Mol Biol* **14**, 15-22
6. Lebreton, A., Tomecki, R., Dziembowski, A., and Seraphin, B. (2008) Endonucleolytic RNA cleavage by a eukaryotic exosome. *Nature* **456**, 993-996
7. Briggs, M. W., Burkard, K. T., and Butler, J. S. (1998) Rrp6p, the yeast homologue of the human PM-Scl 100-kDa autoantigen, is essential for efficient 5.8 S rRNA 3' end formation. *J Biol Chem* **273**, 13255-13263
8. Allmang, C., Kufel, J., Chanfreau, G., Mitchell, P., Petfalski, E., and Tollervey, D. (1999) Functions of the exosome in rRNA, snoRNA and snRNA synthesis. *EMBO J* **18**, 5399-5410
9. Allmang, C., Petfalski, E., Podtelejnikov, A., Mann, M., Tollervey, D., and Mitchell, P. (1999) The yeast exosome and human PM-Scl are related complexes of 3' → 5' exonucleases. *Genes Dev* **13**, 2148-2158
10. Burkard, K. T., and Butler, J. S. (2000) A nuclear 3'-5' exonuclease involved in mRNA degradation interacts with Poly(A) polymerase and the hnRNA protein Npl3p. *Mol Cell Biol* **20**, 604-616
11. Jin, R., Dobry, C. J., McCown, P. J., and Kumar, A. (2008) Large-scale analysis of yeast filamentous growth by systematic gene disruption and overexpression. *Mol Biol Cell* **19**, 284-296
12. Gonzales-Zubiate, F. A., Okuda, E. K., Da Cunha, J. P. C., and Oliveira, C. C. (2017) Identification of karyopherins involved in the nuclear import of RNA exosome subunit Rrp6 in *Saccharomyces cerevisiae*. *J Biol Chem* **292**, 12267-12284
13. Fatica, A., and Tollervey, D. (2002) Making ribosomes. *Curr Opin Cell Biol* **14**, 313-318
14. Kressler, D., Linder, P., and de La Cruz, J. (1999) Protein trans-acting factors involved in ribosome biogenesis in *Saccharomyces cerevisiae*. *Mol Cell Biol* **19**, 7897-7912
15. Mitchell, P., Petfalski, E., Shevchenko, A., Mann, M., and Tollervey, D. (1997) The exosome: a conserved eukaryotic RNA processing complex containing multiple 3' → 5' exoribonucleases. *Cell* **91**, 457-466
16. Zhang, L., Wu, C., Cai, G., Chen, S., and Ye, K. (2016) Stepwise and dynamic assembly of the earliest precursors of small ribosomal subunits in yeast. *Genes Dev* **30**, 718-732
17. Gasse, L., Flemming, D., and Hurt, E. (2015) Coordinated Ribosomal ITS2 RNA Processing by the Las1 Complex Integrating Endonuclease, Polynucleotide Kinase, and Exonuclease Activities. *Mol Cell* **60**, 808-815
18. Konikkat, S., and Woolford, J. L., Jr. (2017) Principles of 60S ribosomal subunit assembly emerging from recent studies in yeast. *Biochem J* **474**, 195-214
19. Fromm, L., Falk, S., Flemming, D., Schuller, J. M., Thoms, M., Conti, E., and Hurt, E. (2017) Reconstitution of the complete pathway of ITS2 processing at the pre-ribosome. *Nat Commun* **8**, 1787
20. Dez, C., Houseley, J., and Tollervey, D. (2006) Surveillance of nuclear-restricted pre-ribosomes within a subnucleolar region of *Saccharomyces cerevisiae*. *EMBO J* **25**, 1534-1546
21. Choque, E., Schneider, C., Gadal, O., and Dez, C. (2018) Turnover of aberrant pre-40S pre-ribosomal particles is initiated by a novel endonucleolytic decay pathway. *Nucleic Acids Res* **46**, 4699-4714

22. Darriere, T., Pilsli, M., Sarthou, M. K., Chauvier, A., Genty, T., Audibert, S., Dez, C., Leger-Silvestre, I., Normand, C., Henras, A. K., Kwapisz, M., Calvo, O., Fernandez-Tornero, C., Tschochner, H., and Gadad, O. (2019) Genetic analyses led to the discovery of a super-active mutant of the RNA polymerase I. *PLoS Genet* **15**, e1008157
23. Huh, W. K., Falvo, J. V., Gerke, L. C., Carroll, A. S., Howson, R. W., Weissman, J. S., and O'Shea, E. K. (2003) Global analysis of protein localization in budding yeast. *Nature* **425**, 686-691
24. Zanchin, N. I., and Goldfarb, D. S. (1999) Nip7p interacts with Nop8p, an essential nucleolar protein required for 60S ribosome biogenesis, and the exosome subunit Rrp43p. *Mol Cell Biol* **19**, 1518-1525
25. Suel, K. E., Gu, H., and Chook, Y. M. (2008) Modular organization and combinatorial energetics of proline-tyrosine nuclear localization signals. *PLoS Biol* **6**, e137
26. Lee, C., Hodgins, D. C., Calvert, J. G., Welch, S. K., Jolie, R., and Yoo, D. (2006) The nuclear localization signal of the PRRS virus nucleocapsid protein viral replication in vitro and antibody response in vivo. *Adv Exp Med Biol* **581**, 145-148
27. Suel, K. E., and Chook, Y. M. (2009) Kap104p imports the PY-NLS-containing transcription factor Tfg2p into the nucleus. *J Biol Chem* **284**, 15416-15424
28. Fries, T., Betz, C., Sohn, K., Caesar, S., Schlenstedt, G., and Bailer, S. M. (2007) A novel conserved nuclear localization signal is recognized by a group of yeast importins. *J Biol Chem* **282**, 19292-19301
29. Graham, A. C., Davis, S. M., and Andrulis, E. D. (2009) Interdependent nucleocytoplasmic trafficking and interactions of Dis3 with Rrp6, the core exosome and importin-alpha3. *Traffic* **10**, 499-513
30. Mamolen, M., Smith, A., and Andrulis, E. D. (2010) Drosophila melanogaster Dis3 N-terminal domains are required for ribonuclease activities, nuclear localization and exosome interactions. *Nucleic Acids Res* **38**, 5507-5517
31. Ho, Y., Gruhler, A., Heilbut, A., Bader, G. D., Moore, L., Adams, S. L., Millar, A., Taylor, P., Bennett, K., Boutilier, K., Yang, L., Wolting, C., Donaldson, I., Schandorff, S., Shewnarane, J., Vo, M., Taggart, J., Goudreault, M., Muskat, B., Alfarano, C., Dewar, D., Lin, Z., Michalickova, K., Willems, A. R., Sassi, H., Nielsen, P. A., Rasmussen, K. J., Andersen, J. R., Johansen, L. E., Hansen, L. H., Jespersen, H., Podtelejnikov, A., Nielsen, E., Crawford, J., Poulsen, V., Sorensen, B. D., Matthiesen, J., Hendrickson, R. C., Gleeson, F., Pawson, T., Moran, M. F., Durocher, D., Mann, M., Hogue, C. W., Figeys, D., and Tyers, M. (2002) Systematic identification of protein complexes in *Saccharomyces cerevisiae* by mass spectrometry. *Nature* **415**, 180-183
32. Krogan, N. J., Cagney, G., Yu, H., Zhong, G., Guo, X., Ignatchenko, A., Li, J., Pu, S., Datta, N., Tikuisis, A. P., Punna, T., Peregrin-Alvarez, J. M., Shales, M., Zhang, X., Davey, M., Robinson, M. D., Paccanaro, A., Bray, J. E., Sheung, A., Beattie, B., Richards, D. P., Canadien, V., Lalev, A., Mena, F., Wong, P., Starostine, A., Canete, M. M., Vlasblom, J., Wu, S., Orsi, C., Collins, S. R., Chandran, S., Haw, R., Rilstone, J. J., Gandi, K., Thompson, N. J., Musso, G., St Onge, P., Ghanny, S., Lam, M. H., Butland, G., Altaf-Ul, A. M., Kanaya, S., Shilatifard, A., O'Shea, E., Weissman, J. S., Ingles, C. J., Hughes, T. R., Parkinson, J., Gerstein, M., Wodak, S. J., Emili, A., and Greenblatt, J. F. (2006) Global landscape of protein complexes in the yeast *Saccharomyces cerevisiae*. *Nature* **440**, 637-643
33. Aloy, P., Ciccarelli, F. D., Leutwein, C., Gavin, A. C., Superti-Furga, G., Bork, P., Bottcher, B., and Russell, R. B. (2002) A complex prediction: three-dimensional model of the yeast exosome. *EMBO Rep* **3**, 628-635
34. Kilchert, C., Wittmann, S., and Vasiljeva, L. (2016) The regulation and functions of the nuclear RNA exosome complex. *Nat Rev Mol Cell Biol* **17**, 227-239
35. Houseley, J., LaCava, J., and Tollervey, D. (2006) RNA-quality control by the exosome. *Nat Rev Mol Cell Biol* **7**, 529-539
36. Tran, E. J., King, M. C., and Corbett, A. H. (2014) Macromolecular transport between the nucleus and the cytoplasm: Advances in mechanism and emerging links to disease. *Biochim Biophys Acta* **1843**, 2784-2795

37. Drazkowska, K., Tomecki, R., Stodus, K., Kowalska, K., Czarnocki-Cieciura, M., and Dziembowski, A. (2013) The RNA exosome complex central channel controls both exonuclease and endonuclease Dis3 activities in vivo and in vitro. *Nucleic Acids Res* **41**, 3845-3858
38. Makino, D. L., Schuch, B., Stegmann, E., Baumgartner, M., Basquin, C., and Conti, E. (2015) RNA degradation paths in a 12-subunit nuclear exosome complex. *Nature* **524**, 54-58
39. Wang, H. W., Wang, J., Ding, F., Callahan, K., Bratkowski, M. A., Butler, J. S., Nogales, E., and Ke, A. (2007) Architecture of the yeast Rrp44 exosome complex suggests routes of RNA recruitment for 3' end processing. *Proc Natl Acad Sci U S A* **104**, 16844-16849
40. Zinder, J. C., Wasmuth, E. V., and Lima, C. D. (2016) Nuclear RNA Exosome at 3.1 Å Reveals Substrate Specificities, RNA Paths, and Allosteric Inhibition of Rrp44/Dis3. *Mol Cell* **64**, 734-745
41. Das, B., Butler, J. S., and Sherman, F. (2003) Degradation of normal mRNA in the nucleus of *Saccharomyces cerevisiae*. *Mol Cell Biol* **23**, 5502-5515
42. Oliveira, C. C., Gonzales, F. A., and Zanchin, N. I. (2002) Temperature-sensitive mutants of the exosome subunit Rrp43p show a deficiency in mRNA degradation and no longer interact with the exosome. *Nucleic Acids Res* **30**, 4186-4198
43. Zhang, E., Khanna, V., Dacheux, E., Namane, A., Doyen, A., Gomard, M., Turcotte, B., Jacquier, A., and Fromont-Racine, M. (2019) A specialised SKI complex assists the cytoplasmic RNA exosome in the absence of direct association with ribosomes. *EMBO J* **38**, e100640
44. Collart, M. A. (2003) Global control of gene expression in yeast by the Ccr4-Not complex. *Gene* **313**, 1-16
45. Azzouz, N., Panasenko, O. O., Colau, G., and Collart, M. A. (2009) The CCR4-NOT complex physically and functionally interacts with TRAMP and the nuclear exosome. *PLoS One* **4**, e6760
46. Beelman, C. A., Stevens, A., Caponigro, G., LaGrandeur, T. E., Hatfield, L., Fortner, D. M., and Parker, R. (1996) An essential component of the decapping enzyme required for normal rates of mRNA turnover. *Nature* **382**, 642-646
47. Boeck, R., Lapeyre, B., Brown, C. E., and Sachs, A. B. (1998) Capped mRNA degradation intermediates accumulate in the yeast *spb8-2* mutant. *Mol Cell Biol* **18**, 5062-5072
48. Hsu, C. L., and Stevens, A. (1993) Yeast cells lacking 5'→3' exoribonuclease 1 contain mRNA species that are poly(A) deficient and partially lack the 5' cap structure. *Mol Cell Biol* **13**, 4826-4835
49. Raijmakers, R., Schilders, G., and Pruijn, G. J. (2004) The exosome, a molecular machine for controlled RNA degradation in both nucleus and cytoplasm. *Eur J Cell Biol* **83**, 175-183
50. Klinge, S., and Woolford, J. L., Jr. (2019) Ribosome assembly coming into focus. *Nat Rev Mol Cell Biol* **20**, 116-131
51. Rodriguez-Galan, O., Garcia-Gomez, J.J., Kressler, D., and de la Cruz, J. (2015) Immature large ribosomal subunits containing the 7S pre-rRNA can engage in translation in *Saccharomyces cerevisiae*. *RNA Biol.* **12**, 838-846
52. Kornprobst, M., Turk, M., Kellner, N., Cheng, J., Flemming, D., Kos-Braun, I., Kos, M., Thoms, M., Berninghausen, O., Beckmann, R., and Hurt, E. (2016) Architecture of the 90S Pre-ribosome: A Structural View on the Birth of the Eukaryotic Ribosome. *Cell* **166**, 380-393
53. Barandun, J., Hunziker, M., and Klinge, S. (2018) Assembly and structure of the SSU processome—a nucleolar precursor of the small ribosomal subunit. *Curr Opin Struct Biol* **49**, 85-93
54. Thoms, M., Thomson, E., Bassler, J., Gnadig, M., Griesel, S., and Hurt, E. (2015) The Exosome Is Recruited to RNA Substrates through Specific Adaptor Proteins. *Cell* **162**, 1029-1038
55. Cepeda, L. P. P., Bagatelli, F. F. M., Santos, R. M., Santos, M. D. M., Nogueira, F. C. S., and Oliveira, C. C. (2019) The ribosome assembly factor Nop53 controls association of the RNA exosome with pre-60S particles in yeast. *J Biol Chem*
56. Yao, R. W., Xu, G., Wang, Y., Shan, L., Luan, P. F., Wang, Y., Wu, M., Yang, L. Z., Xing, Y. H., Yang, L., and Chen, L. L. (2019) Nascent Pre-rRNA Sorting via Phase Separation Drives the Assembly of Dense Fibrillar Components in the Human Nucleolus. *Mol Cell*

57. Niedenthal, R. K., Riles, L., Johnston, M., and Hegemann, J. H. (1996) Green fluorescent protein as a marker for gene expression and subcellular localization in budding yeast. *Yeast* **12**, 773-786
58. Wang, R., Kamgoue, A., Normand, C., Leger-Silvestre, I., Mangeat, T., and Gadal, O. (2016) High resolution microscopy reveals the nuclear shape of budding yeast during cell cycle and in various biological states. *J Cell Sci* **129**, 4480-4495
59. Laporte, D., Courtout, F., Tollis, S., and Sagot, I. (2016) Quiescent *Saccharomyces cerevisiae* forms telomere hyperclusters at the nuclear membrane vicinity through a multifaceted mechanism involving Esc1, the Sir complex, and chromatin condensation. *Mol Biol Cell* **27**, 1875-1884
60. Ghaemmaghami, S., Huh, W. K., Bower, K., Howson, R. W., Belle, A., Dephoure, N., O'Shea, E. K., and Weissman, J. S. (2003) Global analysis of protein expression in yeast. *Nature* **425**, 737-741
61. Sung, M. K., Ha, C. W., and Huh, W. K. (2008) A vector system for efficient and economical switching of C-terminal epitope tags in *Saccharomyces cerevisiae*. *Yeast* **25**, 301-311
62. Longtine, M. S., McKenzie, A., 3rd, Demarini, D. J., Shah, N. G., Wach, A., Brachat, A., Philippsen, P., and Pringle, J. R. (1998) Additional modules for versatile and economical PCR-based gene deletion and modification in *Saccharomyces cerevisiae*. *Yeast* **14**, 953-961
63. Nguyen Ba, A. N., Pogoutse, A., Provar, N., and Moses, A. M. (2009) NLStradamus: a simple Hidden Markov Model for nuclear localization signal prediction. *BMC Bioinformatics* **10**, 202
64. Bakhrat, A., Baranes, K., Krichevsky, O., Rom, I., Schlenstedt, G., Pietrokovski, S., and Raveh, D. (2006) Nuclear import of ho endonuclease utilizes two nuclear localization signals and four importins of the ribosomal import system. *J Biol Chem* **281**, 12218-12226
65. Ohmayer, U., Gamalinda, M., Sauert, M., Ossowski, J., Poll, G., Linnemann, J., Hierlmeier, T., Perez-Fernandez, J., Kumcuoglu, B., Leger-Silvestre, I., Faubladiere, M., Griesenbeck, J., Woolford, J., Tschochner, H., and Milkereit, P. (2013) Studies on the assembly characteristics of large subunit ribosomal proteins in *S. cerevisiae*. *PLoS One* **8**, e68412
66. Gonzales, F. A., Zanchin, N. I., Luz, J. S., and Oliveira, C. C. (2005) Characterization of *Saccharomyces cerevisiae* Nop17p, a novel Nop58p-interacting protein that is involved in Pre-rRNA processing. *J Mol Biol* **346**, 437-455
67. Bachellier-Bassi, S., Gadal, O., Bourout, G., and Nehrbass, U. (2008) Cell cycle-dependent kinetochore localization of condensin complex in *Saccharomyces cerevisiae*. *J Struct Biol* **162**, 248-259
68. Hellmuth, K., Lau, D. M., Bischoff, F. R., Kunzler, M., Hurt, E., and Simos, G. (1998) Yeast Los1p has properties of an exportin-like nucleocytoplasmic transport factor for tRNA. *Mol Cell Biol* **18**, 6374-6386
69. Berger, A. B., Cabal, G. G., Fabre, E., Duong, T., Buc, H., Nehrbass, U., Olivo-Marin, J. C., Gadal, O., and Zimmer, C. (2008) High-resolution statistical mapping reveals gene territories in live yeast. *Nat Methods* **5**, 1031-1037

Table 1. Plasmids		
Name	Characteristics/ markers	Reference
pFA6-mCherry-HIS3	used for cloning pFA6a-mCherry-KIURA3	(67)
pFA6-GST-KIURA3	used for cloning pFA6a-mCherry-KIURA3	(61)
pFA6-GFP(S65T)-KIURA3	URA3, integrative, C-term GFP	(61)
pRS305-Nup2-tDimer	LEU2, integrative, Nup57-RFP	(Laporte et al., 2016)
pRS305-Nup57-tDimer	LEU2, integrative, Nup57-RFP	(58)
pFA6a-mCherry-KIURA3	URA3, integrative, C-term mCherry	This work
pUN-GFP-Nop1	LEU2, CEN/ARS, GFP-NOP1	(68)
pUN100-mcherry-Nop1	LEU2, CEN/ARS, mCherry-NOP1	(69)
pUG34	HIS3, CEN/ARS, PMET25::yEGFP3	(57)
pUG34-Rrp6	HIS3, CEN/ARS, PMET25:: yEGFP3-RRP6	(12)
pUG34-Rrp41	HIS3, CEN/ARS, PMET25:: yEGFP3-RRP41	This work
pUG34-Rrp43	HIS3, CEN/ARS, PMET25:: yEGFP3-RRP43	This work
pUG34-Rrp44	HIS3, CEN/ARS, PMET25:: yEGFP3-RRP44	This work
pUG34-rrp44(1-985)	HIS3, CEN/ARS, PMET25::yEGFP3-rrp44[1-985]	This work
pUG34-rrp44(1-475)	HIS3, CEN/ARS, PMET25::yEGFP3-rrp44[1-475]	This work
pUG34-rrp44Δ(364-407)	HIS3, CEN/ARS, PMET25::yEGFP3-rrp44Δ[364-407]	This work
pUG34(1-363)(408-895)	HIS3, CEN/ARS, PMET25::yEGFP3-rrp44[1-363][408-895]	This work
pUG34-rrp44(1-218)	HIS3, CEN/ARS, PMET25::yEGFP3-rrp44[1-218]	This work
pUG34-rrp44(263-475)	HIS3, CEN/ARS, PMET25::yEGFP3-rrp44[263-475]	This work
pUG34-rrp44(475-1001)	HIS3, ARS/CEN/ PMET25::yEGFP3-rrp44[475-1001]	This work
pUG34-rrp44(R397A,R398T)	HIS3, CEN/ARS, PMET25::yEGFP3-rrp44[R397A,R398T]	This work
pUG34-rrp44(P187A,Y188A)	HIS3, CEN/ARS, PMET25::yEGFP3-rrp44[P187A,Y188A]	This work
YCplac33-GAL-A-RRP44	URA3,ARS/CEN/ PGAL1::ProtA-RRP44	This work
pGEX4T1	GST, AmpR	GE Healthcare
pET28-KAP95	His::KAP95, KanR	(12)
pET29-SRP1	His::SRP1, KanR	(12)
pGEX-RRP44	GST::RRP44, AmpR	(Bagatelli and Oliveira, unpublished)
pGEMT-easy	lacZ	Promega

Table 2. Yeast strains		
Name	Genotype	Reference
<i>RRP41-TAP</i>	<i>MATa his3Δ1 leu2Δ0 met15Δ0 ura3Δ0</i>	(60)
<i>RRP6-TAP</i>	<i>MATa his3Δ1 leu2Δ0 met15Δ0 ura3Δ0</i>	(60)
<i>RRP43-TAP</i>	<i>MATa his3Δ1 leu2Δ0 met15Δ0 ura3Δ0</i>	(60)
<i>RPA190-mCherry (OGT8-1a)</i>	<i>MATa his3Δ1 leu2Δ0 met15Δ0 ura3Δ0 RPA190-mCherry-URA3(K1)</i>	This work
<i>BY4742</i>	<i>MATa his3Δ1 leu2Δ0 lys2Δ0 ura3Δ0</i>	EUROSCARF
<i>BY4742 - Nup57 tDimer (yEO4-1a)</i>	<i>MATa his3Δ1 leu2Δ0 lys2Δ0 ura3Δ0 NUP57-tDimer-LEU2</i>	This work
<i>Rrp6-GFP (yEO9-1a)</i>	<i>MATa his3Δ1 leu2Δ0 met15Δ0 ura3Δ0 Rrp6 GFP-URA3</i>	This work
<i>Rrp6-mCherry (yOE10-1a)</i>	<i>MATa his3Δ1 leu2Δ0 met15Δ0 ura3Δ0 Rrp6 mCherry-URA3</i>	This work
<i>Rrp41-GFP (yOE11-1a)</i>	<i>MATa his3Δ1 leu2Δ0 met15Δ0 ura3Δ0 Rrp41 GFP-URA3</i>	This work
<i>Rrp41-mCherry (yOE12-1a)</i>	<i>MATa his3Δ1 leu2Δ0 met15Δ0 ura3Δ0 Rrp41 mCherry-URA3</i>	This work
<i>Rrp43-GFP (yOE13-1a)</i>	<i>MATa his3Δ1 leu2Δ0 met15Δ0 ura3Δ0 Rrp43 GFP-URA3</i>	This work
<i>Rrp43-mCherry (yOE14-1a)</i>	<i>MATa his3Δ1 leu2Δ0 met15Δ0 ura3Δ0 Rrp43 mCherry-URA3</i>	This work
<i>Rrp44-GFP (yOE15-1a)</i>	<i>MATa his3Δ1 leu2Δ0 met15Δ0 ura3Δ0 Rrp44 GFP-URA3</i>	This work
<i>Rrp44-mCherry (yOE16-1a)</i>	<i>MATa his3Δ1 leu2Δ0 met15Δ0 ura3Δ0 Rrp44 mCherry-URA3</i>	This work
<i>Rrp6-GFP-RPA190mCherry (yOE17-1a)</i>	<i>MATa his3Δ1 leu2Δ0 met15Δ0 ura3Δ0 Rrp6 GFP-URA3 RPA190mCherry-HIS3</i>	This work
<i>Rrp41-GFP RPA190mCherry (yOE18-1a)</i>	<i>MATa his3Δ1 leu2Δ0 met15Δ0 ura3Δ0 Rrp41 GFP-URA3 RPA190mCherry-HIS4</i>	This work
<i>Rrp43-GFP RPA190mCherry (yOE19-1a)</i>	<i>MATa his3Δ1 leu2Δ0 met15Δ0 ura3Δ0 Rrp43 GFP-URA3 RPA190mCherry-HIS5</i>	This work
<i>Rrp44-GFP RPA190mCherry (yOE20-1a)</i>	<i>MATa his3Δ1 leu2Δ0 met15Δ0 ura3Δ0 Rrp44 GFP-URA3 RPA190mCherry-HIS6</i>	This work
<i>BY4741</i>	<i>MATa his3Δ1 leu2Δ0 met15Δ0 ura3Δ0</i>	Euroscarf
<i>Δsrp1 (FGY-41)</i>	<i>YNL189w::kanMX4; his3Δ1; leu2Δ0; lys2Δ0; ura3Δ0; Ycplac33-GAL-A-SRPI</i>	(12)
<i>Δkap95 (FGY-53)</i>	<i>YLR347c::kanMX4; his3Δ1; leu2Δ0; lys2Δ0; ura3Δ0; Ycplac33-GAL-A-KAP95</i>	(12)
<i>Δrrp6 (FGY-88)</i>	<i>BY4742; Mat a; his3Δ1; leu2Δ0; lys2Δ0; ura3Δ0; YOR001w::kanMX4</i>	EUROSCARF
<i>Δrrp44 (2n) (FGY-62)</i>	<i>BY4743; MATa/MATa; ura3Δ0/ura3Δ0; leu2Δ0/leu2Δ0; his3Δ1/his3Δ1;</i>	EUROSCARF

	<i>met15Δ0/MET15; LYS2/lys2Δ0; YOL021c/YOL021c::kanMX4</i>	
<i>Δrrp44/YCplac33-GAL::A-RRP44</i> (FGY-90)	<i>ura3Δ0; leu2Δ0; his3Δ1/; met15Δ0/MET15; LYS2/lys2Δ0; YOL021c::kanMX5 YCplac33-GAL-A-RRP44</i>	This work
<i>BY4742</i> (FGY-76)	<i>Mat α; his3Δ1; leu2Δ0; lys2Δ0; ura3Δ0</i>	EUROSCARF
<i>Δsxm1</i> (FGY-86)	<i>BY4742; Mat α; his3Δ1; leu2Δ0; lys2Δ0; ura3Δ0; YDR395w::kanMX4</i>	EUROSCARF
<i>Δkap114</i> (FGY-60)	<i>BY4742; Mat α; his3Δ1; leu2Δ0; 1 lys2Δ0; ura3Δ0; YGL241w::kanMX4</i>	EUROSCARF
<i>Δkap123</i> (FGY-61)	<i>BY4742; Mat α; his3Δ1; leu2Δ0; lys2Δ0; ura3Δ0; YER110C::kanMX4</i>	EUROSCARF

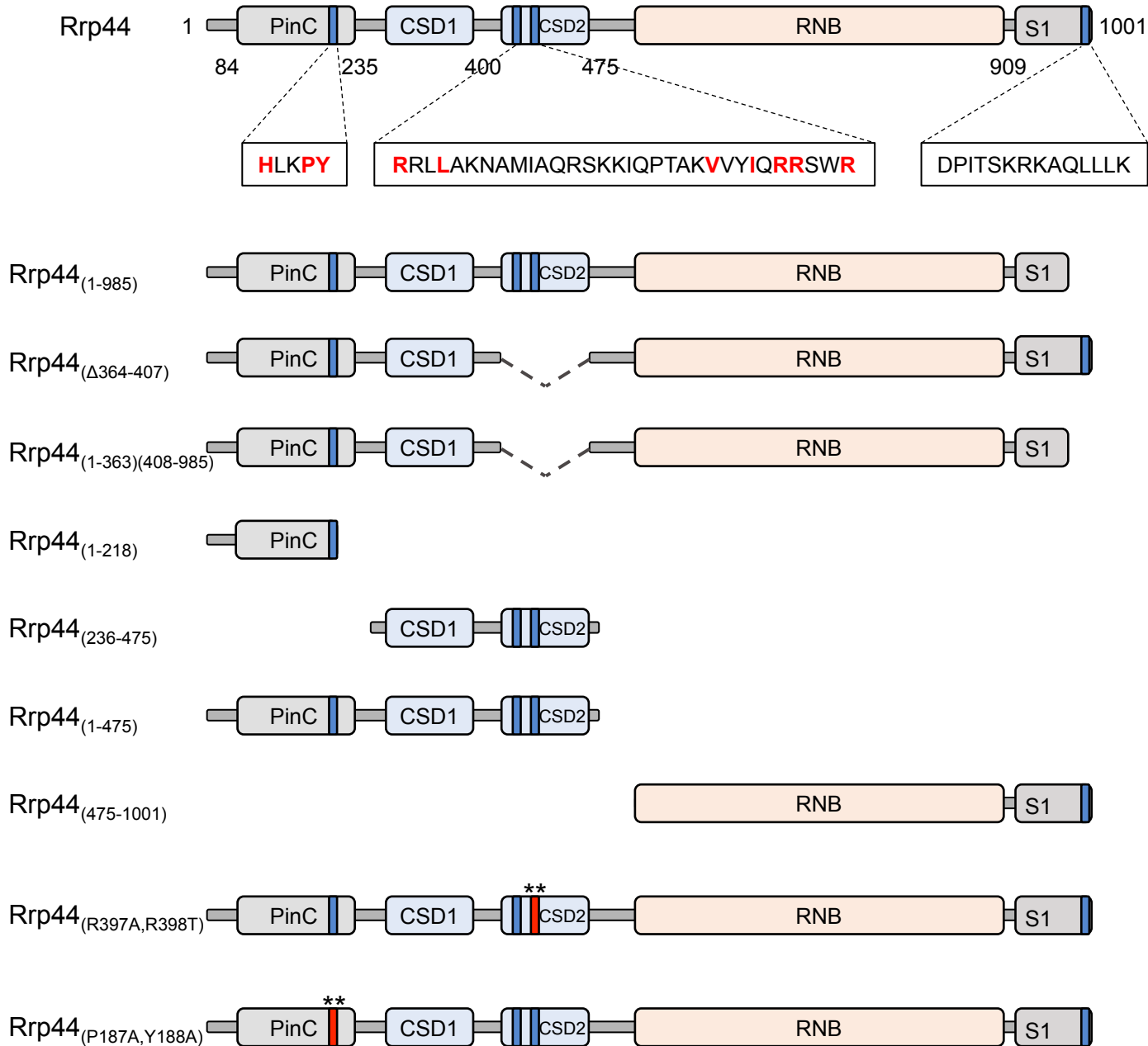


Figure 1

Schematic representation of the deletion and point mutants of Rrp44. Structural and catalytic domains of Rrp44 are shown. Positions of putative NLS are shown in blue and their sequences are highlighted. Asterisks over NLS in red indicate the positions of the point mutations.

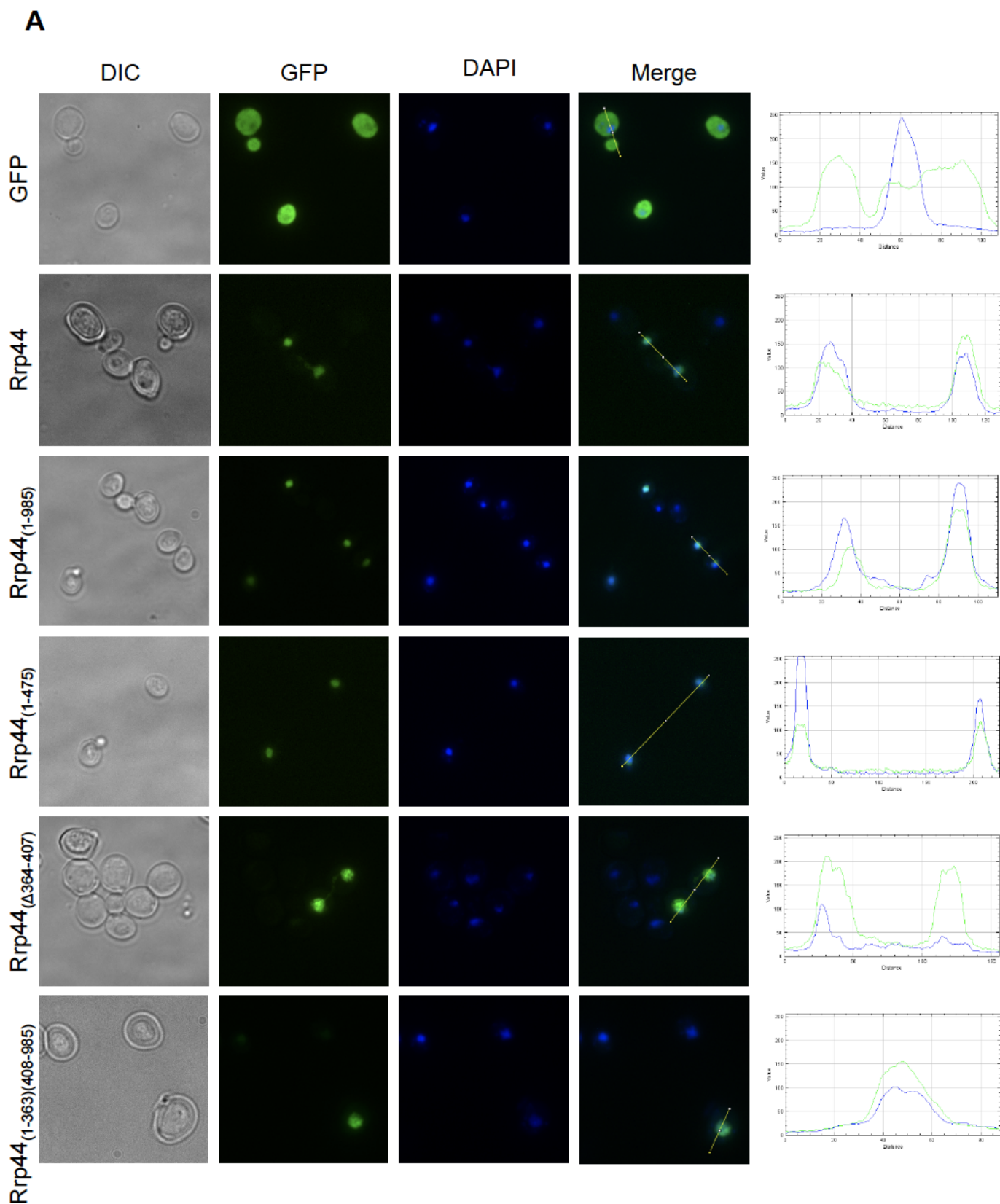


Figure 2

NLS1 is the most important region for Rrp44 nuclear import. Fluorescence microscopy images show the subcellular localization of the Rrp44 mutants expressed in wild type cells. (A) GFP, GFP-Rrp44, Rrp44₁₋₉₈₅, Rrp44₁₋₄₇₅, Rrp44_{Δ364-407}, Rrp44₍₁₋₃₆₃₎₍₄₀₈₋₉₈₅₎; (B) Rrp44₁₋₂₁₈, Rrp44₂₃₆₋₄₇₅, Rrp44₄₇₅₋₁₀₀₁, Rrp44_{R397A,R398A}, Rrp44_{P187A,Y188A}. Analysis of GFP-Rrp44 relative to DAPI using ImageJ is shown on the right. Cells expressing Rrp44₁₋₂₁₈ show two phenotypes, both depicted here, with this mutant localized to the nucleus of 67% of cells, and present in aggregates in 30% of cells. GFP-Rrp44 relative to DAPI by using ImageJ is shown on the right. Green lines represent GFP and blue lines represent DAPI. Images were acquired and edited separately. Quantification of different phenotypes is shown in Fig. S3.

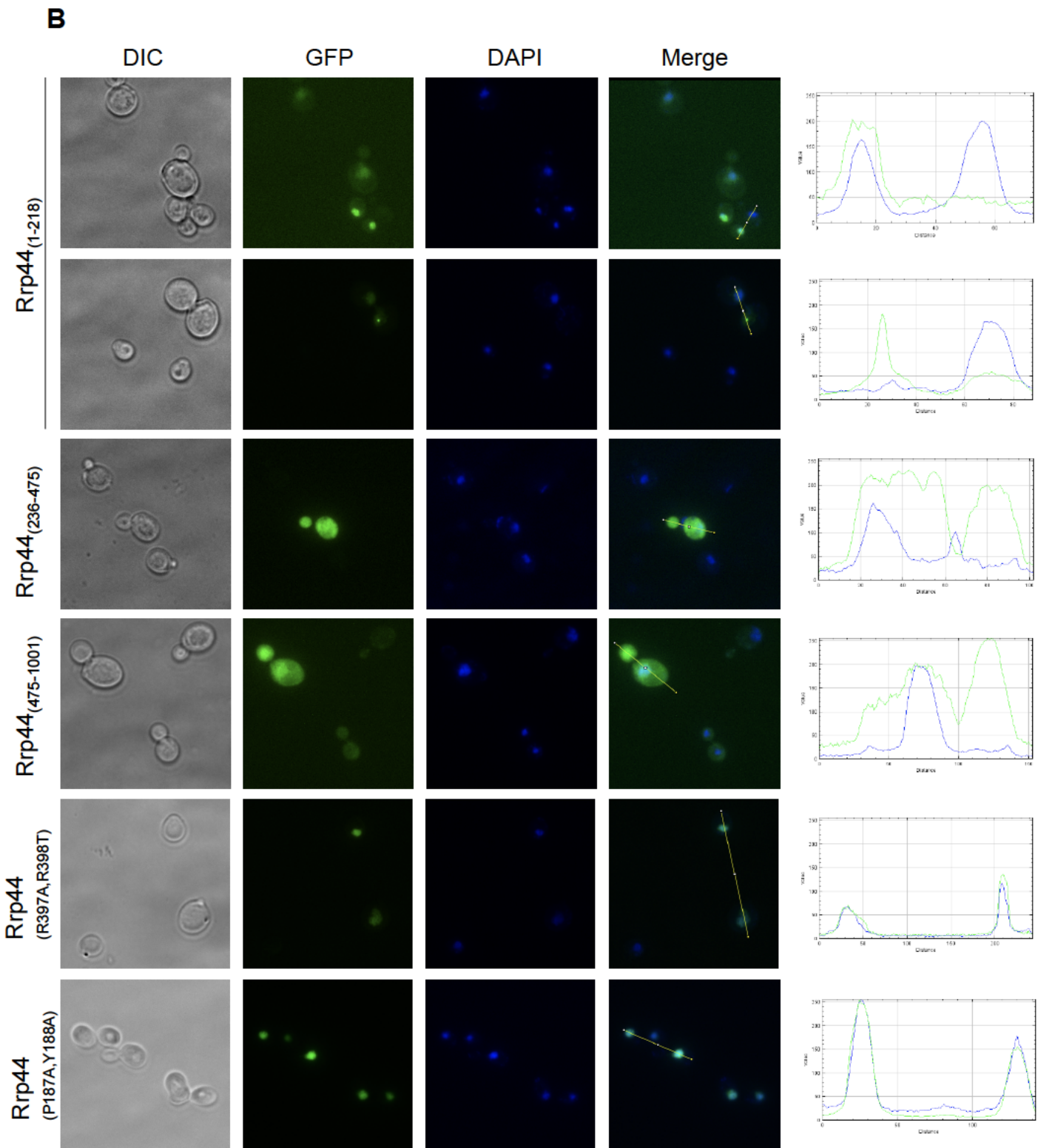


Figure 2

NLS1 is the most important region for Rrp44 nuclear import. Fluorescence microscopy images show the subcellular localization of the Rrp44 mutants expressed in wild type cells. (A) GFP, GFP-Rrp44, Rrp44₁₋₉₈₅, Rrp44₁₋₄₇₅, Rrp44_{Δ364-407}, Rrp44₍₁₋₃₆₃₎₍₄₀₈₋₉₈₅₎; (B) Rrp44₁₋₂₁₈, Rrp44₂₃₆₋₄₇₅, Rrp44₄₇₅₋₁₀₀₁, Rrp44_{R397A, R398A}, Rrp44_{P187A, Y188A}. Analysis of GFP-Rrp44 relative to DAPI using ImageJ is shown on the right. Cells expressing Rrp44₁₋₂₁₈ show two phenotypes, both depicted here, with this mutant localized to the nucleus of 67% of cells, and present in aggregates in 30% of cells. GFP-Rrp44 relative to DAPI by using ImageJ is shown on the right. Green lines represent GFP and blue lines represent DAPI. Images were acquired and edited separately. Quantification of different phenotypes is shown in Fig. S3.

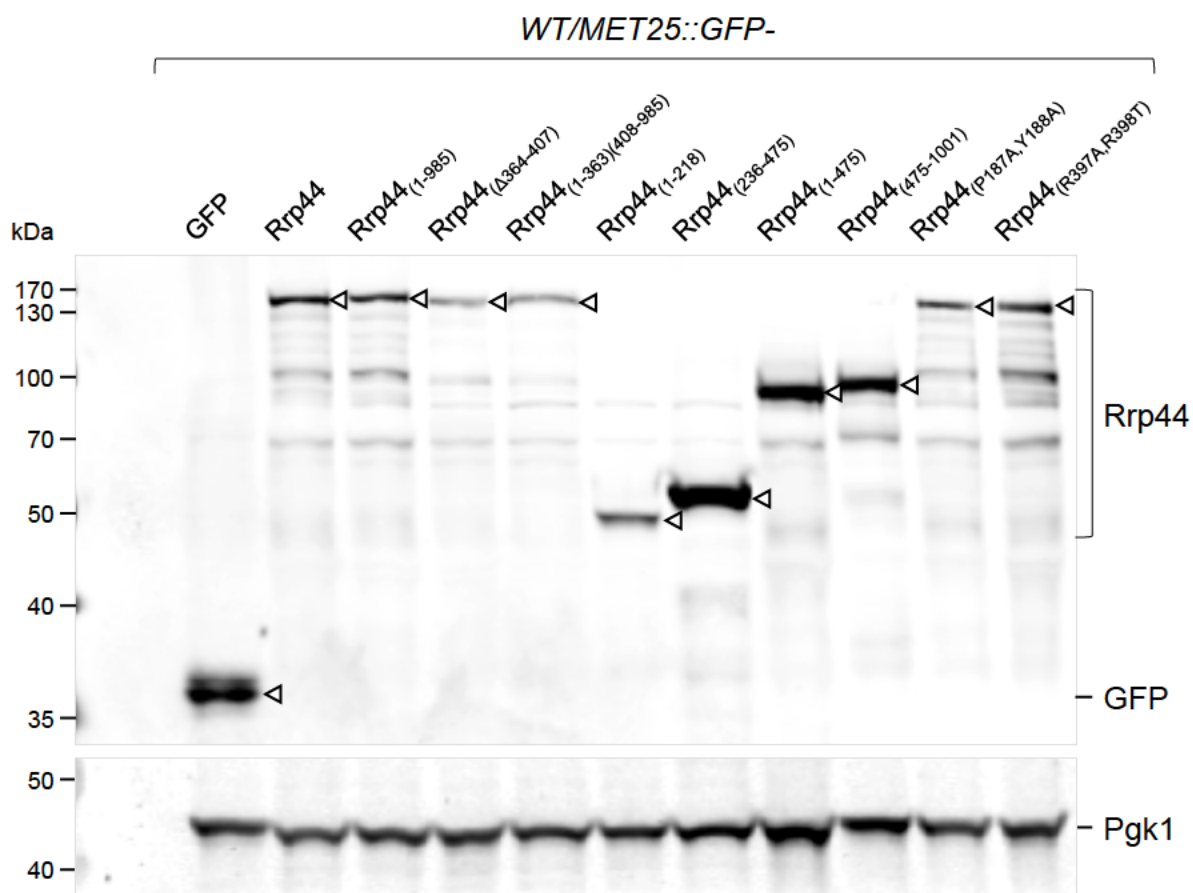


Figure 3

Expression of episomal Rrp44 mutants in wild type cells. Western blot for the determination of the expression levels of the GFP-Rrp44 mutants in BY4742 strain. Total cell extracts were separated by SDS-PAGE and subjected to western blot with antibodies against GFP and Pgk1, used here as an internal control. Arrowheads indicate the positions of the respective bands. In this 10% acrylamide gel, deletion mutants Rrp44_{Δ364-407} and Rrp44₍₁₋₃₆₃₎₍₄₀₈₋₉₈₅₎ run similar to full-length Rrp44. 8% gel is shown in Fig. S4A.

Δrrp44/GAL::RRP44/MET25::GFP-

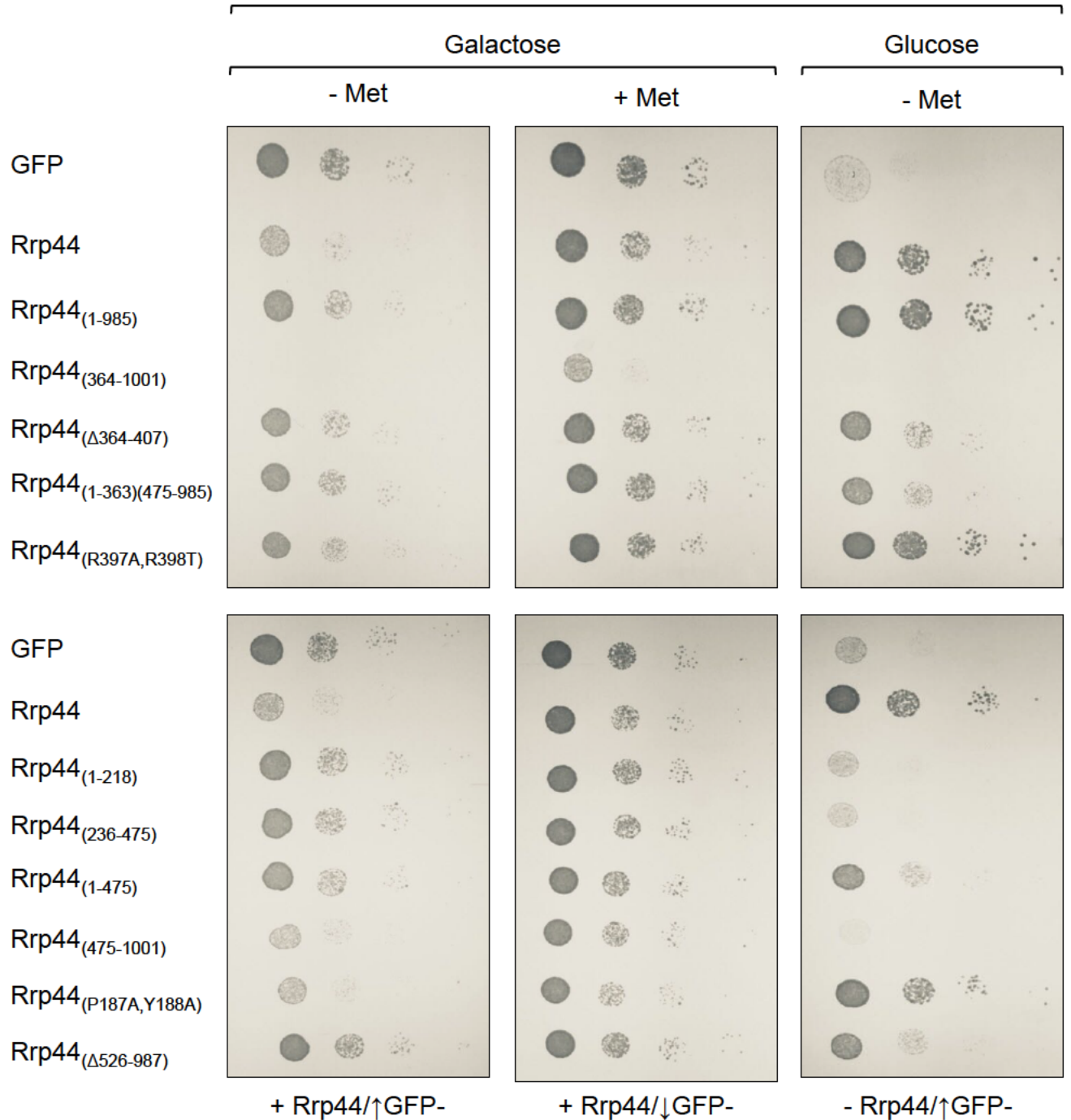


Figure 4

Analysis of growth of conditional strain *Δrrp44/GAL::RRP44* expressing Rrp44 mutants. Conditional strain was transformed with plasmids containing the Rrp44 mutants under control of *MET25* promoter, and incubated in galactose (expression of WT Rrp44) or glucose (expression of Rrp44 mutants) medium, in the presence or absence of methionine (lower and higher levels of the mutants, respectively). Mutants Rrp44_{Δ364-407} and Rrp44₍₁₋₃₆₃₎₍₄₀₈₋₉₈₅₎ partially complement growth in glucose, whereas Rrp44₁₋₉₈₅, Rrp44_{R397A,R398A} and Rrp44_{P187A,Y188A} fully complement growth in glucose, although overexpression of the latter inhibits growth in galactose.

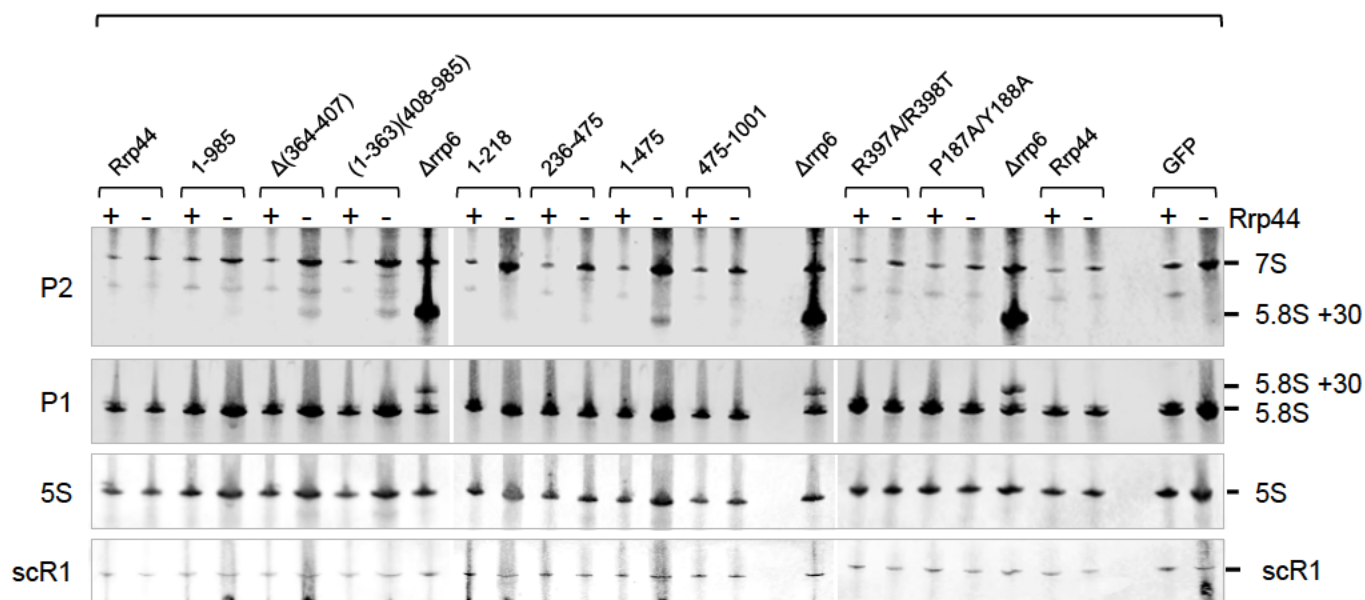
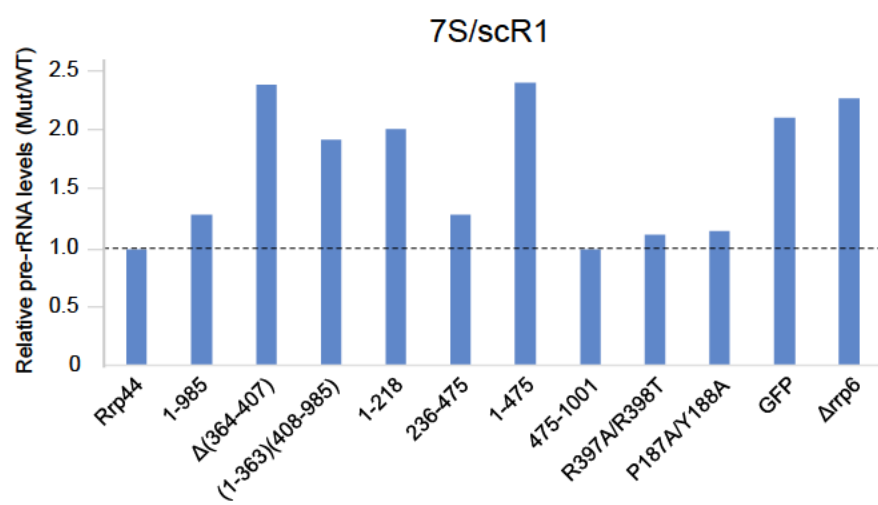
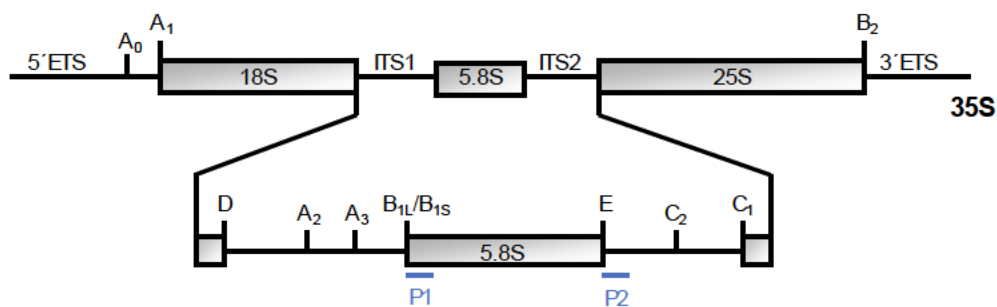
A*Δrrp44/GAL::RRP44/MET25::GFP-***B****C**

Figure 5

Analysis pre-rRNA processing in Rrp44 mutants. Northern hybridization of total RNA extracted from *Δrrp44/GAL::RRP44/MET25::GFP*- strains growing either in galactose (+ WT Rrp44), or glucose (- WT Rrp44) medium, and separated by electrophoresis on denaturing polyacrylamide gels. Precursor and mature rRNAs detected with the different probes are indicated on the right. 5S rRNA and scR1 were used as controls of RNAs not processed by the exosome. A representative of three independent experiments is shown. **(B)** Quantification of the bands detected by northern hybridization. Signals of pre-rRNA 7S were corrected for scR1 signals and plot shows the levels of 7S in the mutants relative to Rrp44 growing in glucose. **(C)** Schematic representation of the yeast 35S pre-rRNA indicating the hybridizing positions of the probes.

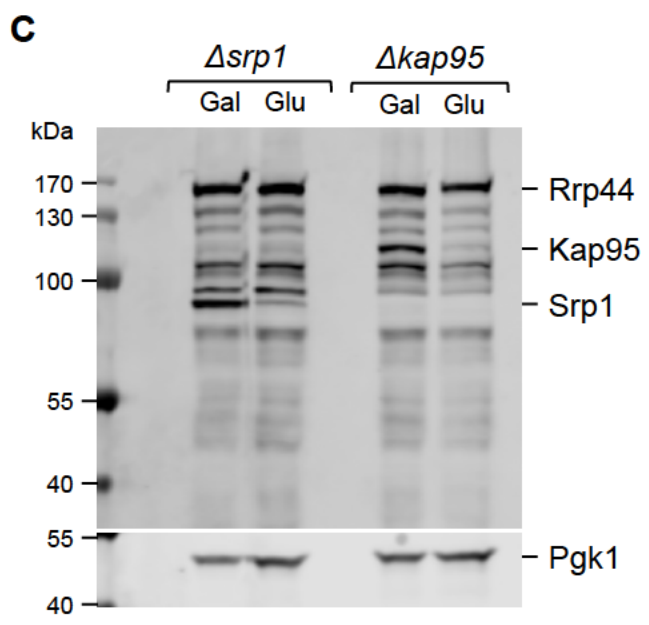
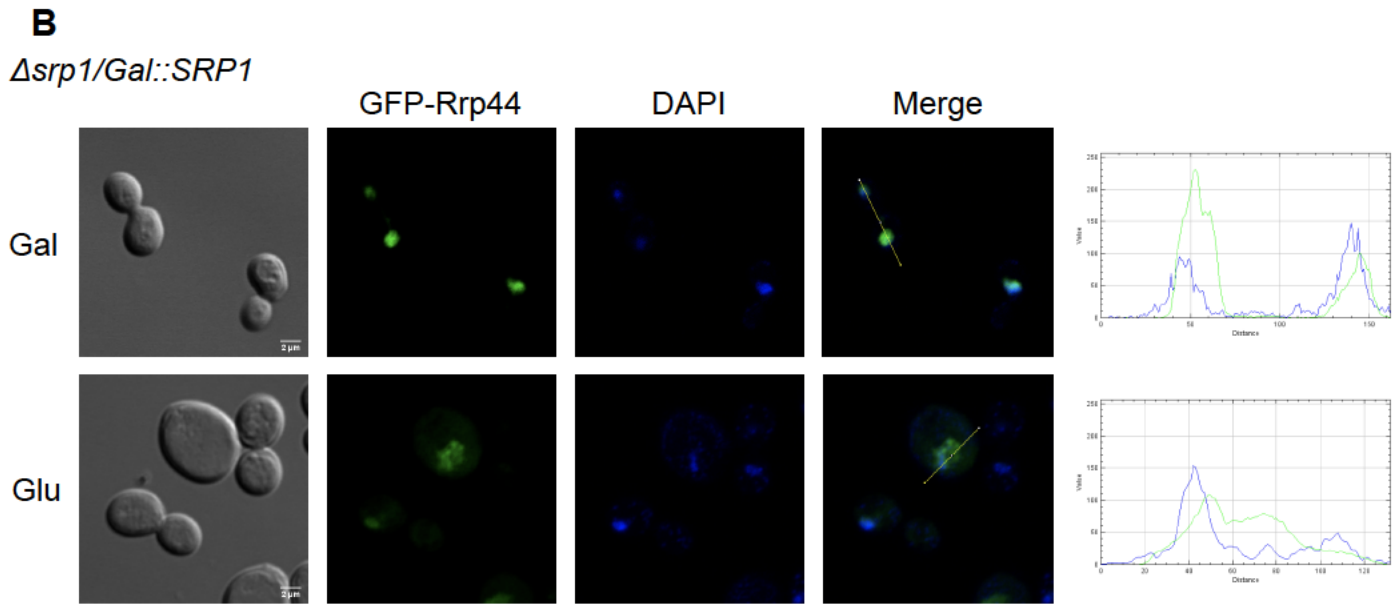
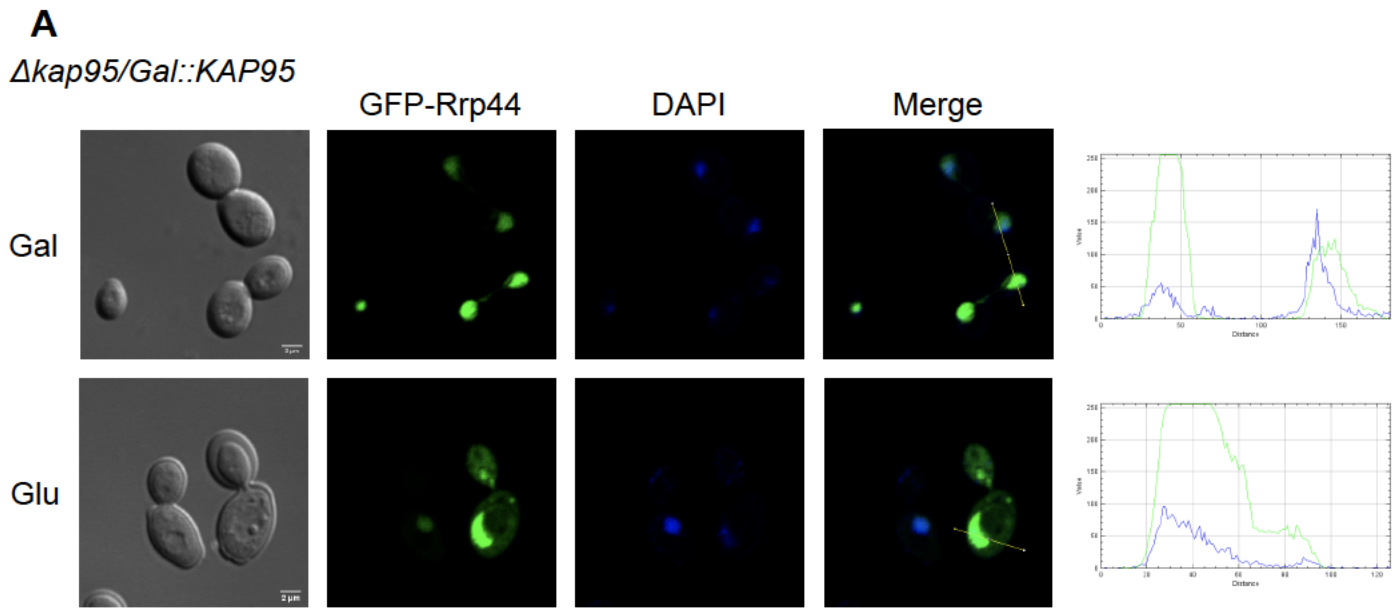


Figure 6

Figure 6

Inhibition of karyopherins expression affects the subcellular localization of GFP-Rrp44. **(A)** Laser scanning confocal microscope images show the subcellular localization of GFP-Rrp44 after inhibition of Kap95 expression in glucose medium in $\Delta kap95/GAL::KAP95$ cells. GFP-Rrp44 relative to DAPI by using ImageJ is shown on the right. Green lines represent GFP and blue lines represent DAPI. **(B)** Analysis of the subcellular localization of GFP-Rrp44 after inhibition of Srp1 expression in glucose medium in $\Delta srp1/GAL::SRP1$ cells. GFP-Rrp44 relative to DAPI is shown on the right. **(C)** Western blot showing the repressed expression of the karyopherins in glucose medium.

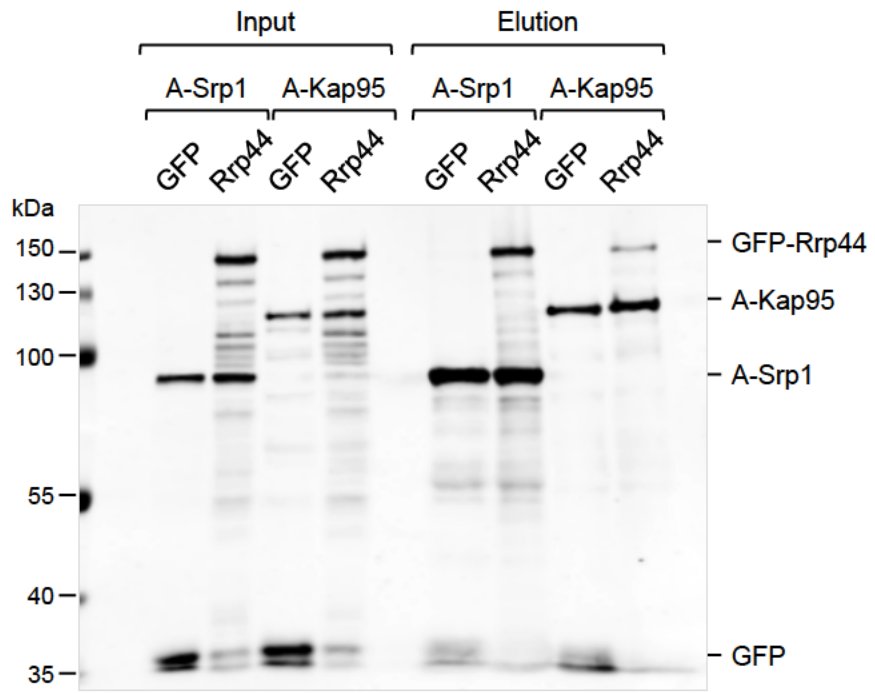
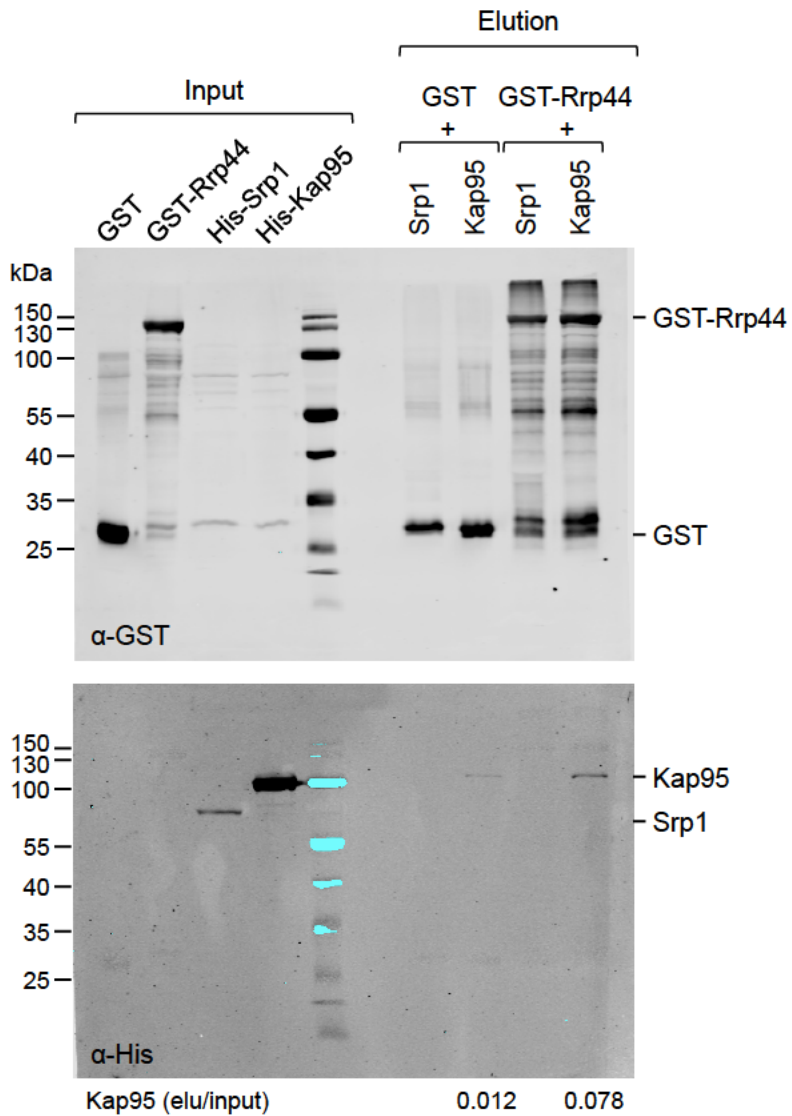
A**B**

Figure 7

Figure 7

Interaction of Rrp44 with karyopherins. **(A)** GFP-Rrp44 co-immunoprecipitates with A-Srp1 and A-Kap95. Yeast strains expressing ProtA-Srp1 or ProtA-Kap95, and GFP or GFP-Rrp44 were used in co-immunoprecipitation experiments. ProtA-Kap95 and ProtA-Srp1 were immobilized on IgG-sepharose beads, and co-immunoprecipitated proteins were analyzed by western blot with antibody against GFP. Input and elution fractions are shown. GFP-Rrp44 is co-immunoprecipitated with both karyopherins. **(B)** GST-Rrp44 pulls-down His-Kap95. *E. coli* expressed GST and GST-Rrp44 bound to glutathione-sepharose beads were incubated with His-Srp1, or His-Kap95-containing extracts. After washing, bound proteins were eluted with glutathione and analyzed by western blot. **Numbers below indicate the quantification of the Kap95 signal in the elution fractions relative to the input.** The same membrane was incubated with antibodies against GST and His tags. Saturated marker signals appear as bluish bands at 800 nm (lower panel). Figure shown is representative of three independent experiments.

$\Delta rrp44/GAL::A\text{-}RRP44/GFP\text{-}$

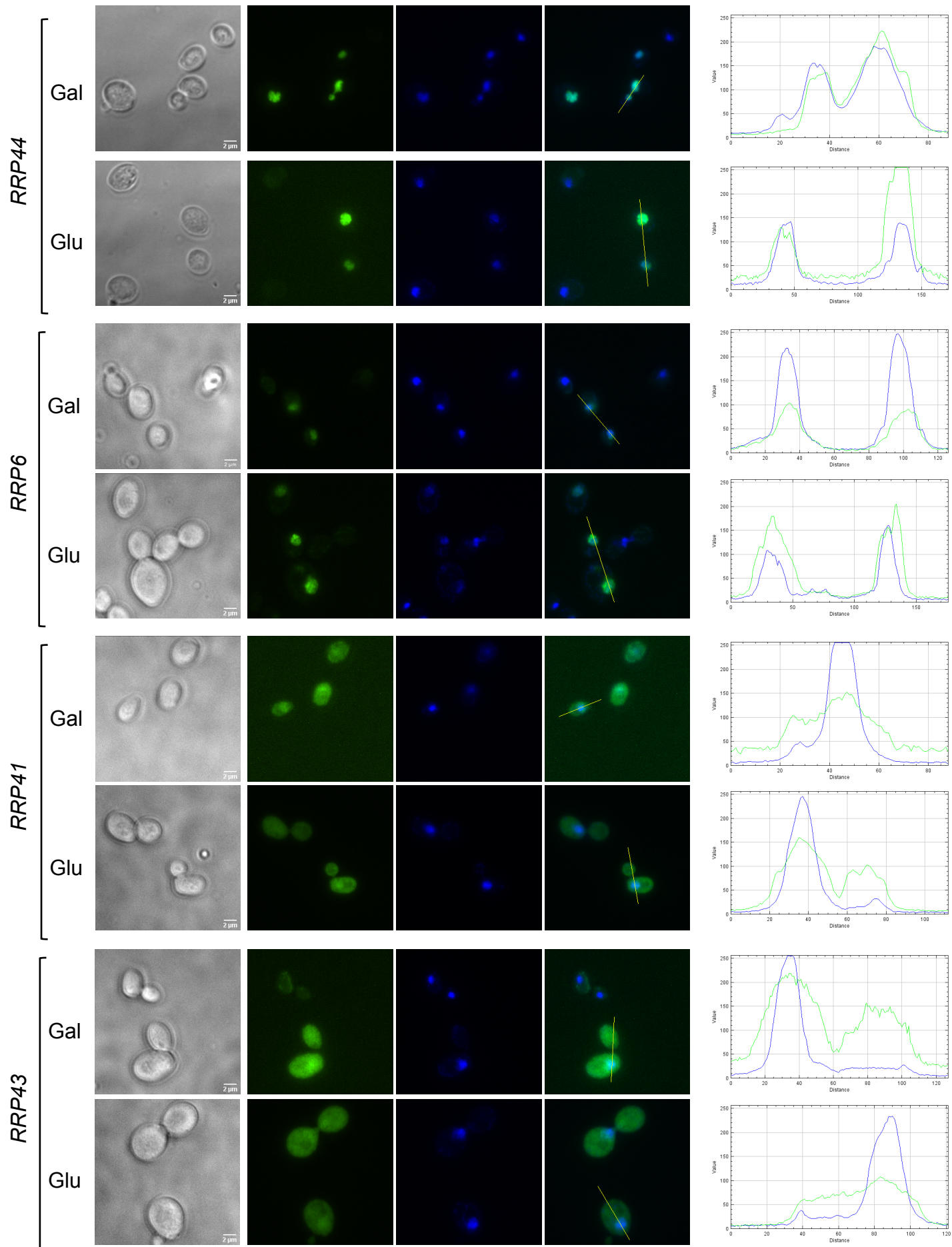


Figure 8

Figure 8

Depletion of Rrp44 does not affect subcellular localization of core exosome subunits Rrp41 and Rrp43. *Δrrp44/GAL::RRP44* was transformed with plasmids expressing GFP-fused exosome subunits Rrp44, Rrp6, Rrp41 and Rrp43 and incubated in media containing either galactose (Rrp44 expression), or glucose (Rrp44 repression). All four exosome subunits are concentrated in the nucleus, although Rrp41 and Rrp43 are also visible in the cytoplasm. Images were acquired and edited separately. [GFP-fused proteins relative to DAPI by using ImageJ is shown on the right](#). Green lines represent GFP and blue lines represent DAPI.

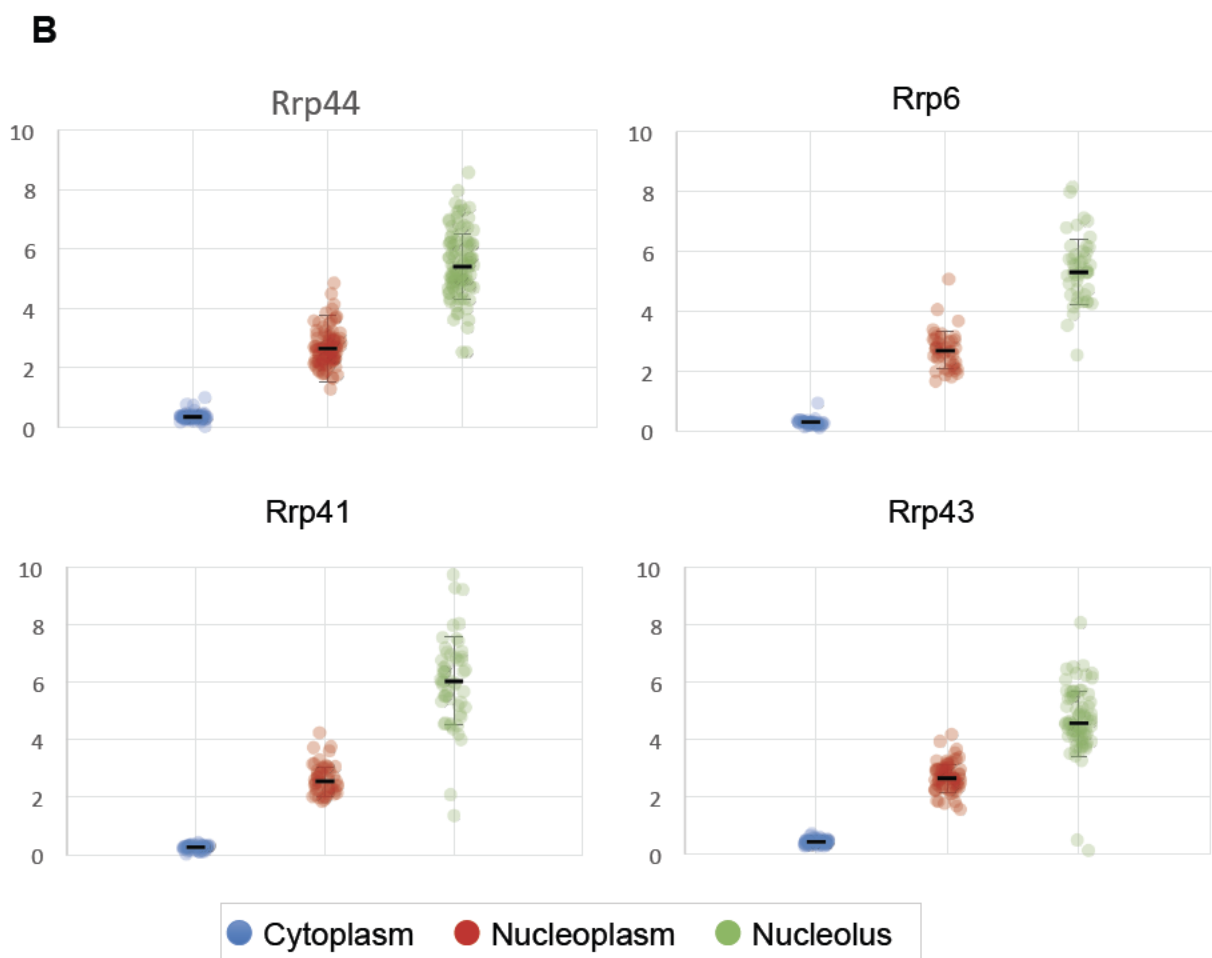
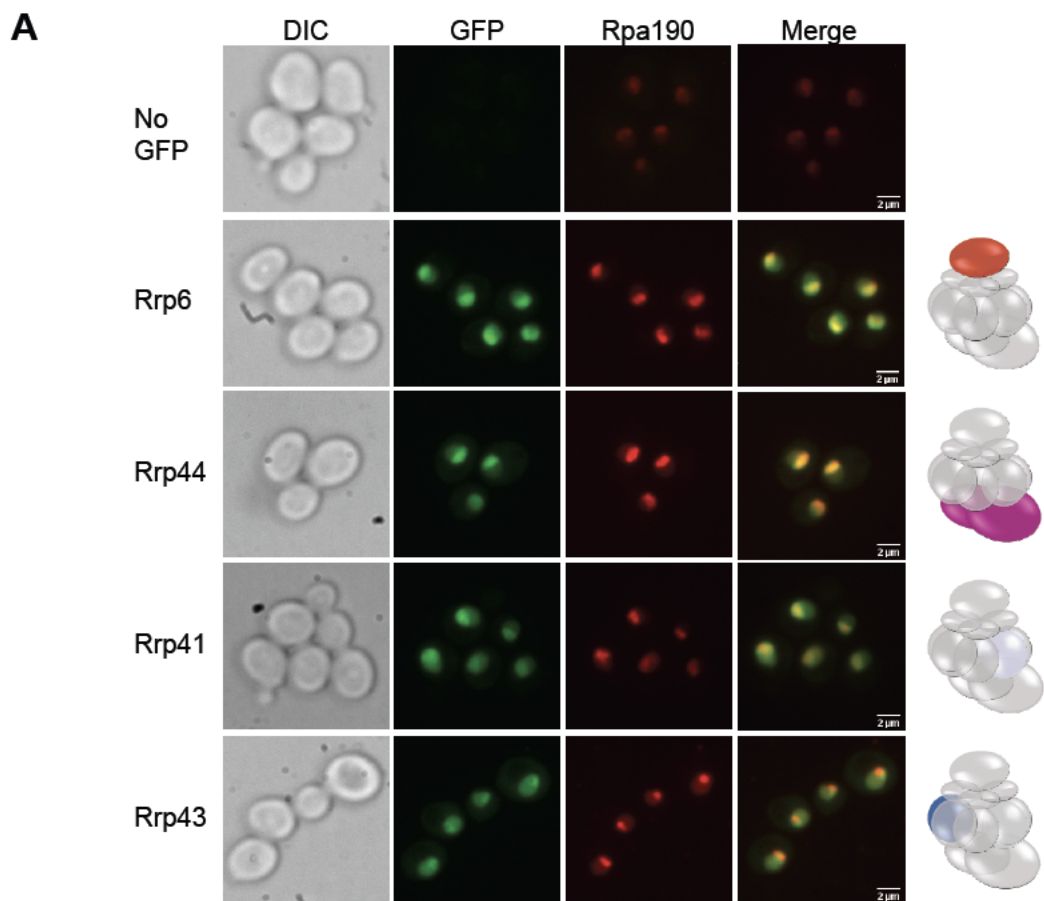


Figure 9

Figure 9

Endogenously expressed GFP-fused exosome subunits localize to the nucleolus. (A) Z-projection of high-resolution spinning-disk laser scanning confocal microscope images show the subcellular localization of GFP-tagged exosome subunits. Rpa190-mCherry was used as nucleolar marker. (B) Exosome subunits enrichment in different cell compartments. We calculated the enrichment of the GFP tagged exosome subunits signals in each compartment over an homogeneous distribution of the cellular signal. For that, we calculated the mean intensity of each compartment and divided this value by the computed mean intensity (total cell signal/total cell surface). Blue dots represent cytoplasm enrichment, red dots represent nucleoplasm and green dots represent nucleolus.

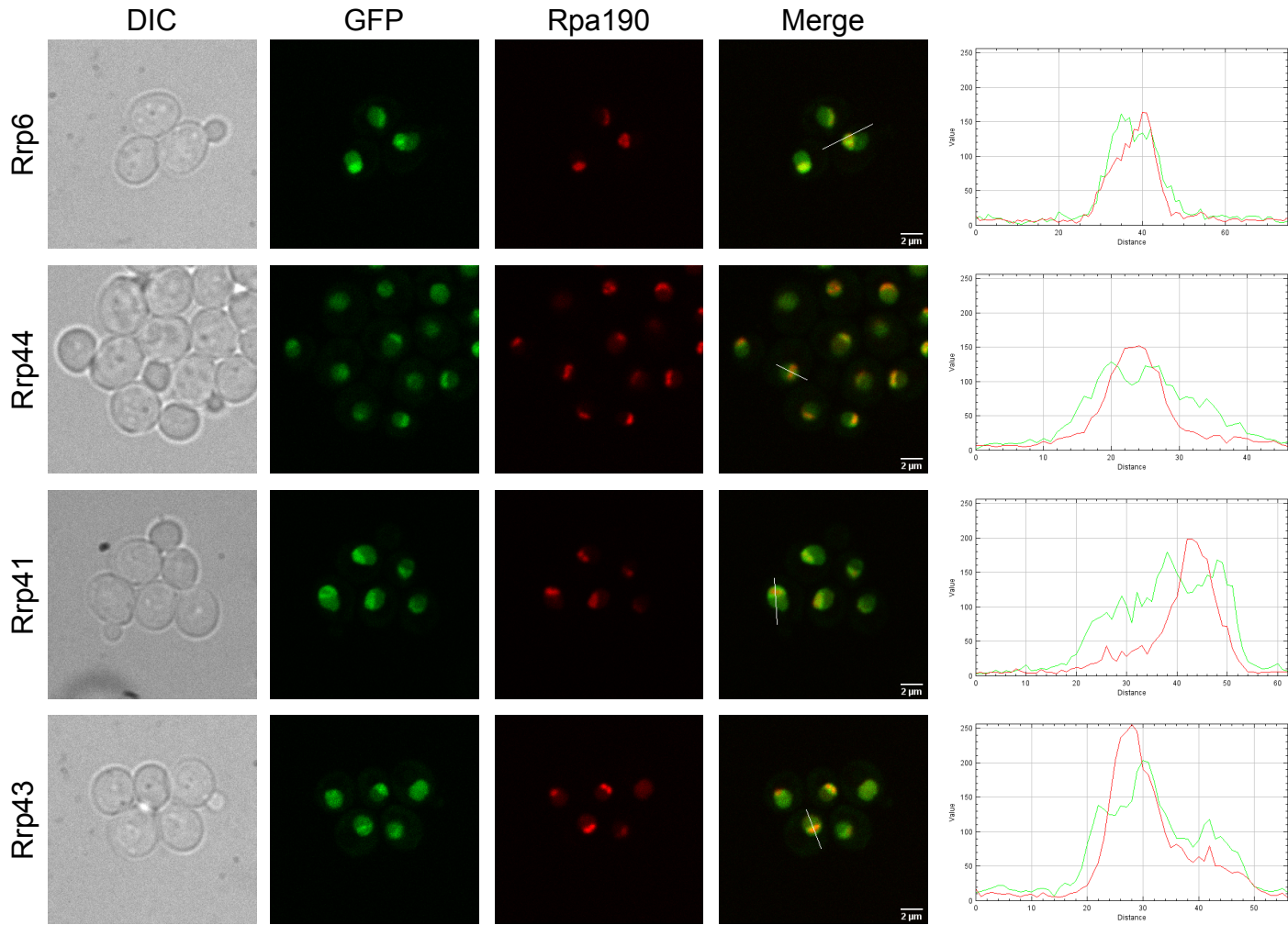


Figure 10

Exosome subunits do not co-localize exactly with nucleolar RNA polymerase I subunit Rpa190. GFP-tagged images obtained by Z-section of spinning disk confocal microscope shows that exosome subunits have slightly different localization from Rpa190-mCherry, used as nucleolar marker. Note that single Z-step images are different from Z-projected images, which shows the sum of all detected signal of cells.